

## User Manual

### Operation of the Turnkey Phase Doppler

### Interferometer (TK-PDI)

### Spray Drop Size and Velocity Measurement



TK1 and TK2 PDI Systems

## Table of Contents

Chapter 1 .....	1
Preface.....	1
Chapter 2.....	2
Before You Start.....	2
Chapter 3.....	3
Artium Technologies, Inc .....	3
Chapter 4.....	4
Warranty.....	4
Chapter 5.....	6
About this Manual.....	6
Chapter 6.....	7
Laser Safety .....	7
Chapter 7 .....	9
Hardware Set-up/Connection .....	9
Descriptions of the Connections .....	10
TK-PDI Mounting Options.....	13
Purge Air for TK body .....	15
Purge Hoods/Beam Shields.....	16
Chapter 8.....	19
Software Set-up.....	19
Menus .....	24
AIMSScript .....	40
Traverse Simple Node Paths.....	41
Creating an AIMSScript Program.....	44
Plotting Data Versus Traverse Position .....	48

AIMS Troubleshooting .....52  
Moving AIMS to Another Computer .....55  
AIMS Preferred Units and Formatting .....59  
  
Optics Cleaning ..... 61  
  
Sizing Air Bubbles in Water ..... 63  
  
Appendix I ..... 70  
    PDI Calculations .....70  
  
Appendix II ..... 82  
    Phase Doppler Interferometry Theory of Operation .....82  
  
Appendix III ..... 95  
    Bibliography .....95

## Chapter 1

### *Preface*

Thank you for your system purchase. We are confident that this product will serve you well. Any comments you may have concerning this product or your application are encouraged. Please feel free to contact us at:

**Artium Technologies, Inc.**  
470 Lakeside Drive, Unit C  
Sunnyvale, CA 94085 USA  
Tel: (408) 737-2364  
Fax: (408) 737-2374  
E-mail: [info@artium.com](mailto:info@artium.com)  
Website: [www.artium.com](http://www.artium.com)

This manual is designed to be comprehensive and easy-to-understand. However, should you be uncertain about how to do certain things, or the consequences of doing something, feel free to contact us at **Artium Technologies, Inc.** We will be happy to answer any questions you may have. Also, if you have any comments on improving this manual, we would appreciate hearing from you.

## Chapter 2

### *Before You Start*

Upon receipt of the instrument, inspect the shipping carton for any significant external damage. Unpack the unit and inspect for internal damage. If any damage is found, immediately notify the shipper and Artium Technologies, Inc.

Retain the shipping carton and packing material. If the instrument ever needs repair, the cartons will ensure safe shipment of the unit to Artium Technologies, Inc.

## Chapter 3

### *Artium Technologies, Inc.*

**Artium Technologies, Inc. (“Artium”)** was established in 1998 to develop advanced instrumentation and to engage in various opportunities associated with laser-based diagnostics for particle field and spray characterization. Since its inception, Artium has been actively involved in conducting research and development, design, manufacture, and sales/marketing of laser-based instrumentation for particle field and spray characterization; for both fundamental research and process/quality control applications. Our instruments have been used in various applications including characterization of sprays used in coating medical devices, cloud measurements for aircraft icing research studies, characterizing sprays in spray combustion, and measuring soot emissions from diesel engines. We have also developed systems for characterizing black carbon for quality control purposes in carbon black production.

Throughout the years, our team has established an excellent record worldwide for providing innovative advanced diagnostics that perform reliably under difficult conditions. Our instruments set the standard for performance and for their capability in producing results.

## Chapter 4

### *Warranty*

Artium Technologies, Inc. ("Artium") warrants products of its manufacture against defective materials and workmanship for a period of thirteen (13) months from the date of shipment to the purchaser. The liability of Artium under this warranty is limited, at Artium's option, solely to repair or replacement with equivalent products, or appropriate credit adjustment not to exceed the sales price to the purchaser, provided that:

1. Artium is notified in writing by the purchaser within the warranty period promptly upon the discovery of defects,
2. The purchaser has obtained a Return Materials Authorization Number ("RMA.") from Artium, which RMA number Artium agrees to provide to the purchaser promptly upon request,
3. The defective products are returned to Artium, in the original packing material or alternate material approved by Artium, with transportation charges prepaid by the purchaser, and
4. Artium's examination of such products discloses to its satisfaction that defects were not caused by mishandling of the product, careless operation of the system, negligence, misuse, improper installation, accident, or unauthorized attempts to repair or perform alterations.

The original warranty period of any product which has been repaired or replaced by Artium shall not thereby be extended.

THE FOREGOING WARRANTY IS PROVIDED EXPRESSLY IN LIEU OF AND **ARTIUM** HEREBY DISCLAIMS ALL OTHER WARRANTIES, EXPRESS OR IMPLIED, INCLUDING ANY WARRANTY OF MERCHANTABILITY OR FITNESS FOR A PARTICULAR PURPOSE, AND OF ALL OTHER OBLIGATIONS OR LIABILITIES ON ARTIUM'S PART, AND ARTIUM NEITHER ASSUMES STORE AUTHORIZES ANY OTHER PERSON TO ASSUME FOR ARTIUM ANY OTHER LIABILITIES.

The foregoing warranty is only valid for Artium products sold within the United States and Canada. For products sold outside of United States and Canada, please refer to the local authorized Artium distributor for applicable warranty terms and conditions.

## LIMITATION OF LIABILITY

The remedies set forth above constitute the sole and exclusive remedies against Artium for the finishing of nonconforming or defective products. In no event, including if the products are nonconforming, effective, delayed, were not delivered, shall Artium be liable for any special contingent, indirect, or consequential damages, even if Artium has been advised of the possibility of such damages, whether under a contract, tort, property, or other legal theory. Such damages for which Artium is not responsible include, but are not limited to, personal-injury, property damage, anticipated profits, labor expended, delays, and loss of use.



## Chapter 6

### *About this Manual*

The purpose of this manual is to provide step-by-step instructions for the proper setup and operation of your instrument.

#### Electrical and Laser Safety

Before attempting to operate the system, users should familiarize themselves, with all aspects of electrical and laser safety and if applicable, ensure that **laser safety glasses are available** to all individuals present when the instrument is operated.

This manual provides a description of the steps required in setting up the system hardware and software, including as applicable:

- Warning and safety label descriptions and placement.
- Diagrams of basic electrical and other electronic connections for the system.
- Proper set up of the electronic system, although the system software is designed to automatically set these parameters reliably.
- Optical parameters required for optimal measurements and the means for selecting these parameters.
- Basic alignment techniques and descriptions.
- Theory of operation.
- Various related algorithms and calculations.

## Chapter 7

### Laser Safety

#### Explanations of Terms

Cautions and Warnings used throughout this manual are explained below. Always read and heed this information. It is basic to the safe and proper operation of the system.

**WARNING:** Hazardous to persons. An action or circumstance which may potentially cause personal injury or loss of life. Mechanical damage may also result.

**CAUTION:** Hazardous to persons or equipment. To disregard the caution may cause mechanical damage, however it is not likely to cause serious injury or death.

#### Safety Summary

The American National Standards Institute publishes a laser safety standard for users titled “American National Standard for the safe use of lasers” (ANSI Z136.1). Artium Technologies, Inc. recommends that laser users obtain and follow the procedures described in this ANSI user standard. Copies may be obtained from:

American National Standards Institute Inc.  
1430 Broadway  
New York, NY 10018

OR

Laser Institute of America  
12524 research Parkway  
Orlando, FL 32826

Please refer to the following publications for additional information on laser safety:

“Safe Use of Lasers” (Z136.1)  
American National Standards Institute (ANSI)  
11<sup>th</sup> West 42<sup>nd</sup> Street  
New York, NY 10036 USA  
(212) 642-4900

“A Guide for Control of Laser Hazards”  
American Conference of Governmental and  
Industrial Hygienists (ACGIH)  
6500 Glenway Avenue, Bldg. D-7  
Cincinnati, OH 45211 USA  
(513) 661-7881

Occupational Safety and Health Administration  
U.S. Department of Labor  
200 Constitution Avenue N.W.  
Washington, DC 20210 USA  
(202) 523-8148

“Safety of Laser Products” (EN60825-1:1994)  
Global Engineering Documents  
15 Iverness Way East  
Englewood, CO 80112-5704 USA  
(303) 792-2181

## Laser Safety Labels

Laser safety labels can be found on various locations both on the outside and inside of the TK-PDI.

**WARNING:** Exposure to laser radiation can be harmful. All apertures which can emit laser energy in excess of levels which are considered safe, or areas of the instrument to which exposure to laser radiation can occur due to disassembly, are identified with the appropriate label shown in this section. Take extreme care when working in areas where these labels are placed.

**WARNING:** Instrument users must provide protective eyewear suitable for the lasers' emission wavelength. The lasers' emission wavelengths are indicated in nanometers (nm). The green laser emits at 532 nm.

**WARNING:** Use of controls or adjustments or performance of procedures other than those specified herein may result in hazardous radiation exposure.

## Laser Safety LABELS USED ON THE TK-PDI

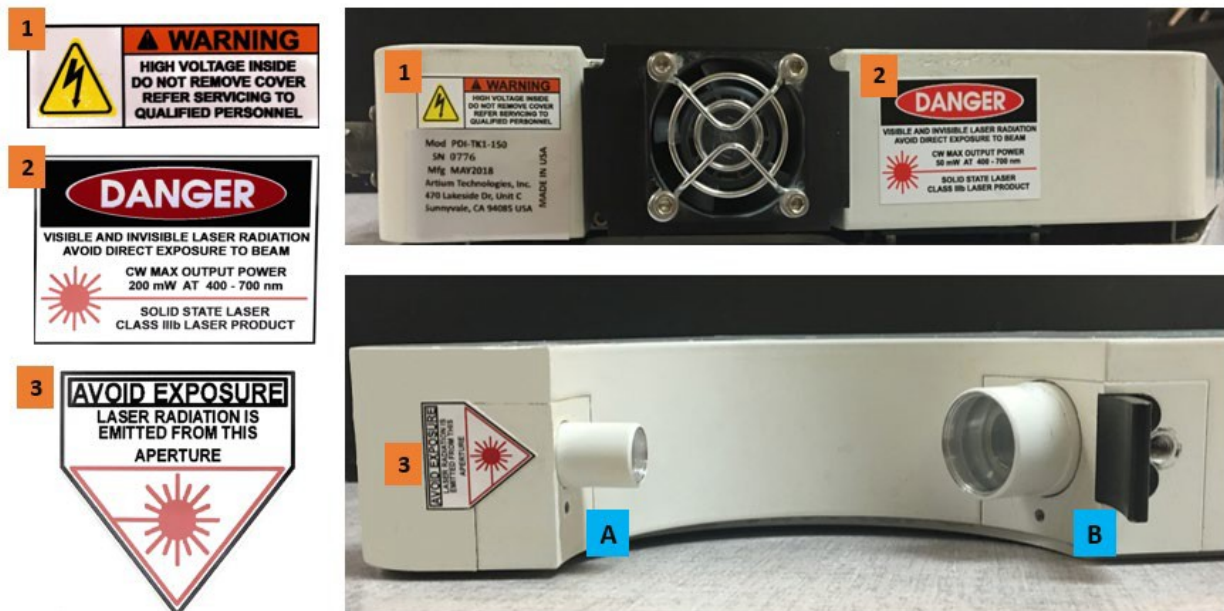


Figure 6.1: Laser beams exit window A and are stopped by beam block B.

## Chapter 7

### Hardware Set-up/Connection

TK-PDI Major Components and connections

- 1) TK-PDI Optical Head
- 2) ASA Signal Processor
- 3) Computer



Figure 7.1: The Artium TK-PDI System.

Figure 7.1 shows the components of the TK-PDI with labels describing each electronics and optics enclosure. A description of the connectors on the electronics and optical enclosures is provided in figure 7.2. In general, the electronic connections can only be made to the proper connectors. However, care must be taken in connecting the signal cables to the proper locations, namely connectors labeled as Input Signals (BNC connectors) on the ASA Signal Processor must be connected to Input 1A, 1B, and 1C with the labeled cables from the receiver cable. Care must be taken to carefully align connectors before plugging them in so that the pins are not damaged or misaligned.



Figure 7.2: Connections for the TK-PDI Instrument.

### ***Descriptions of the Connections***

In this section, each of the connections on the electronics and optical enclosures will be described and will refer to figure 7.2.

#### **1. TK-PDI Cable**

This six-meter cable connects the optical head to the signal processor. The cable includes three raw signal coaxial cables (indicated as 5 in figure 7.2) and communicates the settings and other functions to the signal processor. This cable is indicated as 1 in figure 7.2.

#### **2. High-Speed Data Cable**

Not shown, is the cable that connects the ASA signal processor to the I/O card plugged into the computer. Digitized data is transmitted back to the computer through the high-speed interface card. For ASA2 systems (shown here), the cable is a standard Cat5 ethernet cable. For ASA3 systems, the cable is an optical fiber. This cable connection location is indicated as 2 in Fig. 7.2.

### 3. Interlock

This connector allows a laser interlock switch located on the door or other access to the laboratory to be activated so that when a connection is broken via the interlock switch, the laser will shut off. For the TK system to operate, this circuit must be closed either thru the door switch or with the shorting cap provided. The interlock is indicated as 3 in figure 7.2.

### 4. A/C Adaptor

The system is powered by the included 110-240VAC Input; to 24VDC Output; 120w adaptor. Only use this adaptor or others meeting the same specifications to ensure safe, continued operation of the instrument. The adaptor is indicated as 4 in figure 7.2.

### ASA Signal Processor CH 1

The ASA signal processor accepts the Doppler burst signals from the TK-PDI and amplifies and filters the incoming analog signals, performs digital and analog signal detection, and presents information on the detected digitized signals to the computer via a high-speed interface card. The signals are processed to produce the size and one component of velocity of the droplets. The following connections are required for proper operation of the instrument.

#### Input Signals

The BNC cables provided with the instrument must be connected to the proper BNC connectors on the ASA signal processor. The cables are labeled 1A, 1B, and 1C. The other end of the cable is connected to the TK-PDI enclosure indicated as 5 on Fig. 7.2.

#### RAW A, RAW B, and RAW C BNC Connectors

These connectors are used as monitor points for observing the signals with an oscilloscope. The signals at these points are identical to the signals entering the signal processor at the input signal connectors. It is useful to observe the raw signals with an oscilloscope during alignment of the instrument and during operation to ensure that the quality of the signals is adequate and that there are no problems with the incoming signals.

#### OUT A, OUT B and OUT C BNC Connectors

These monitor points allow the observation of the signals after they have been filtered by the low pass and high pass filters and amplified logarithmically. The signals observable at this point are digitized and that information is passed to the computer for processing using the complex Fourier transform.

#### GATE OUT BNC Connector

This monitor point allows the observation of the gate signal which rises to approximate level of 5 V when a signal is detected and falls at the end of the signal. This information is useful in observing the performance of the Doppler signal burst detection.

## EXTERNAL INPUT

This connection point allows the input of information from other data gathering devices such as pressure monitoring, temperature monitoring, etc. These data are then appended to the data stream being transmitted to the computer for processing. It can also be connected to a resettable clock so that ensemble averages can be obtained from pulsed injections, for example.

**WARNING:** Instrument users must provide protective eyewear suitable for the lasers emission wavelength. The laser emission wavelength is indicated in nanometers (nm). The key in the back of the transmitter enclosure turns the lasers on or off. If the power box is turned Off and On again, the key switch must be turned Off and then On to start the laser.

This enclosure contains the green laser which produces hazardous light beam intensities. Caution must be taken in operating the system and protective eyewear must be used when performing alignment. Enclosure also contains the appropriate optics and a Bragg cell is used to shift the frequency and split each laser beam into two equal intensity beams.

**TK-PDI Mounting Options**

The TK-PDI enclosure can be mounted to an optical table, optical rails, or other supporting fixtures.

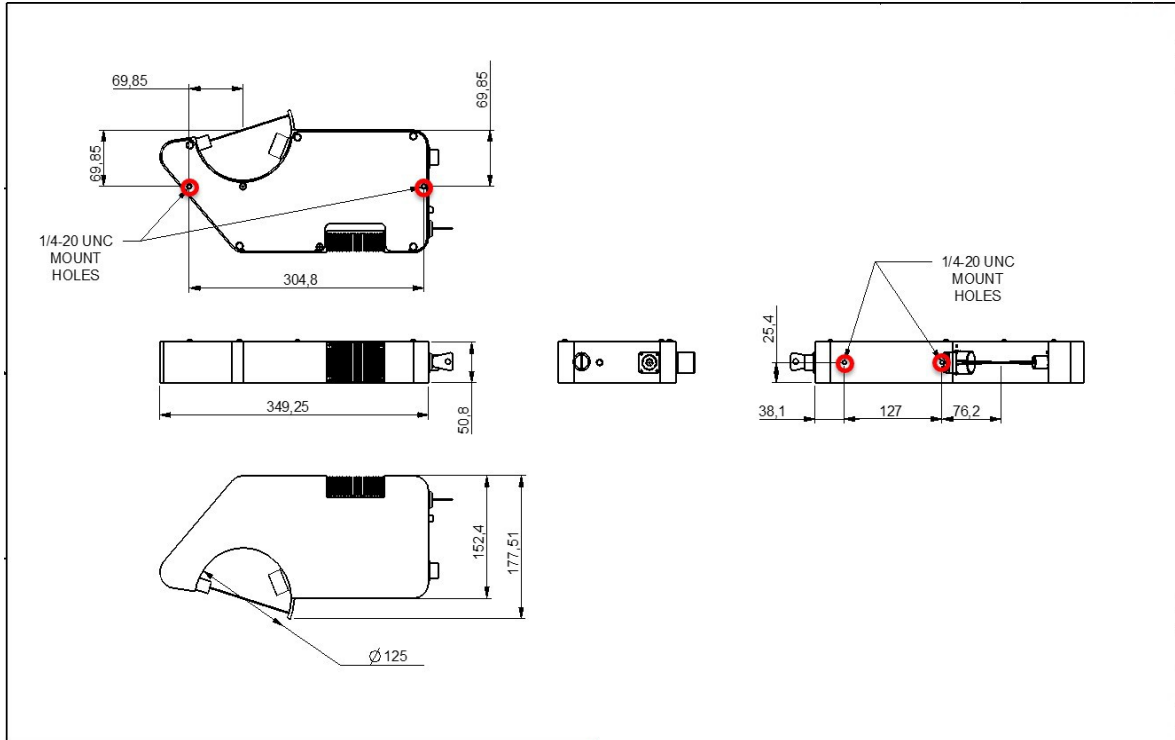


Figure 7.3: Schematic showing the TK1-PDI enclosure mounting holes.

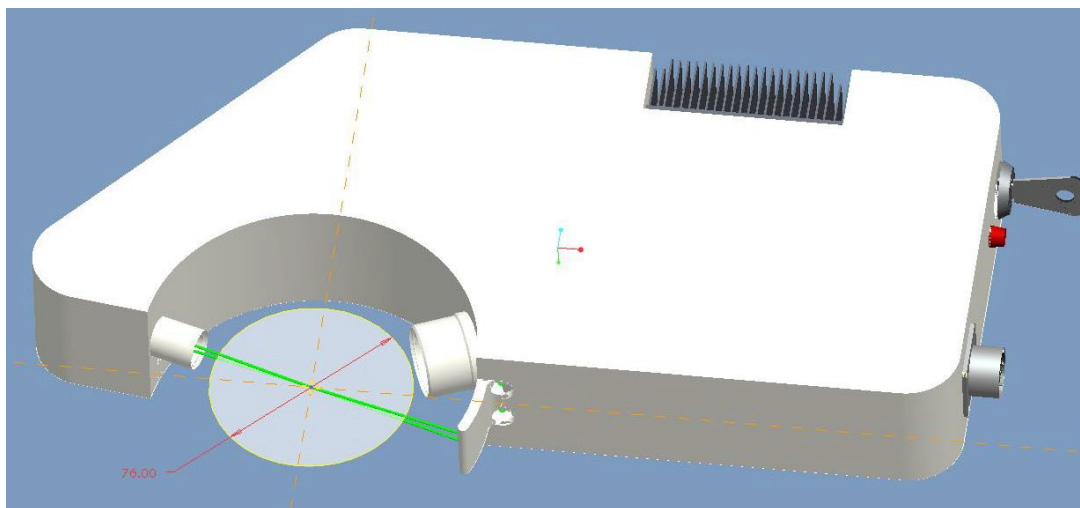


Figure 7.4: Schematic showing the TK1-PDI working distance without purge hoods.



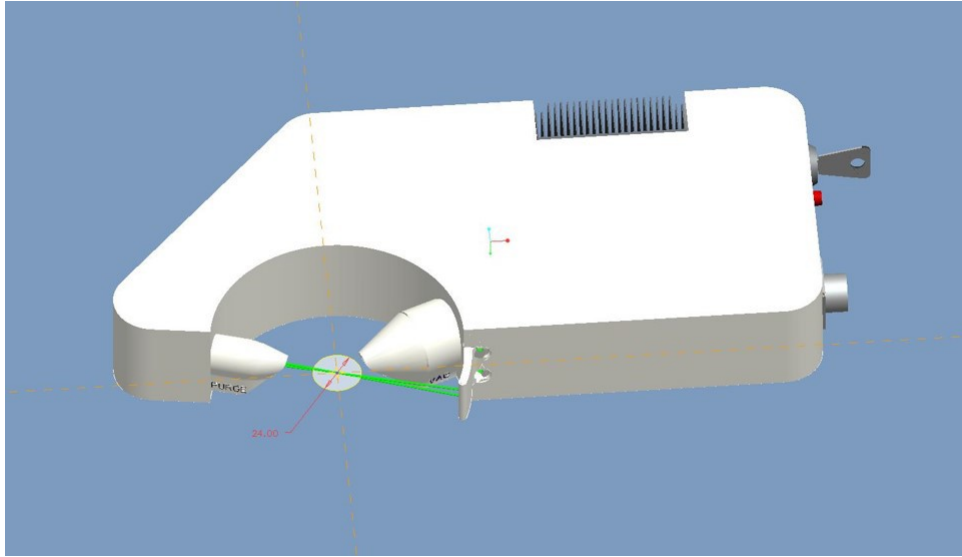


Figure 7.5: Schematic showing the TK1-PDI working distance with purge hoods.

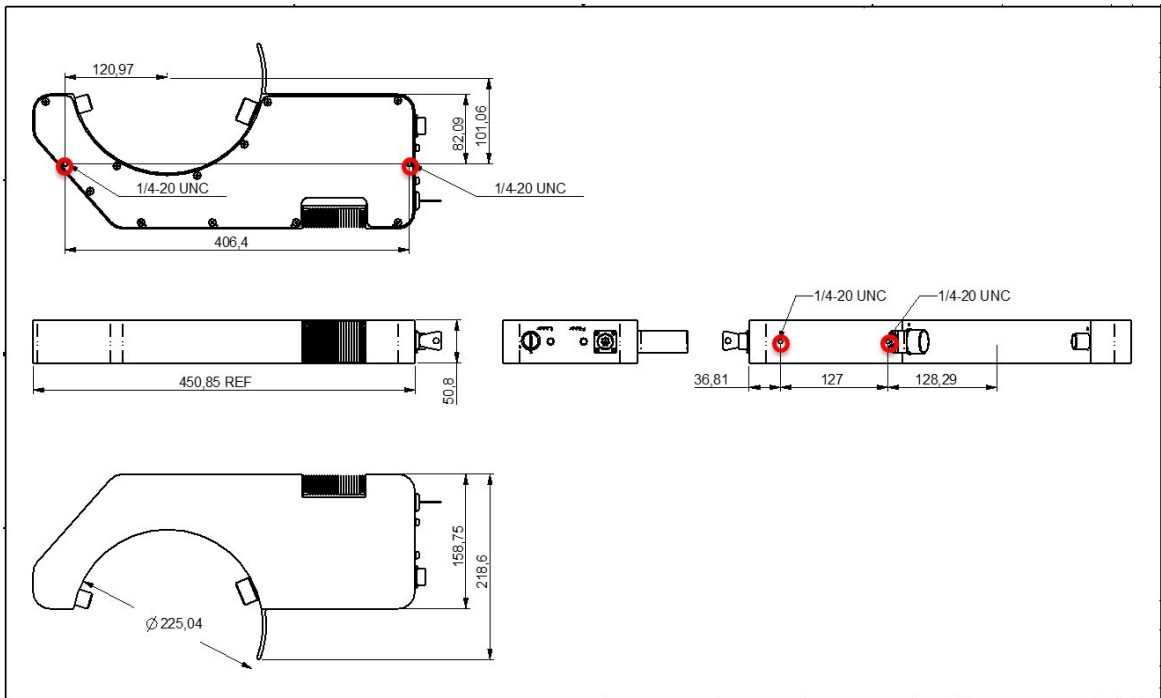


Figure 7.6: Schematic showing the TK2-PDI enclosure mounting holes.

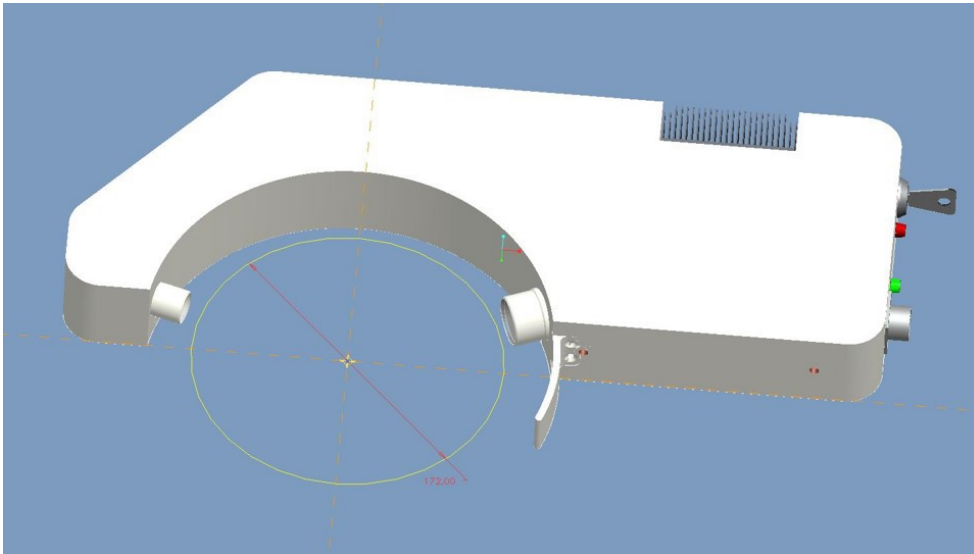


Figure 7.7: Schematic showing the TK2-PDI working distance without purge hoods.

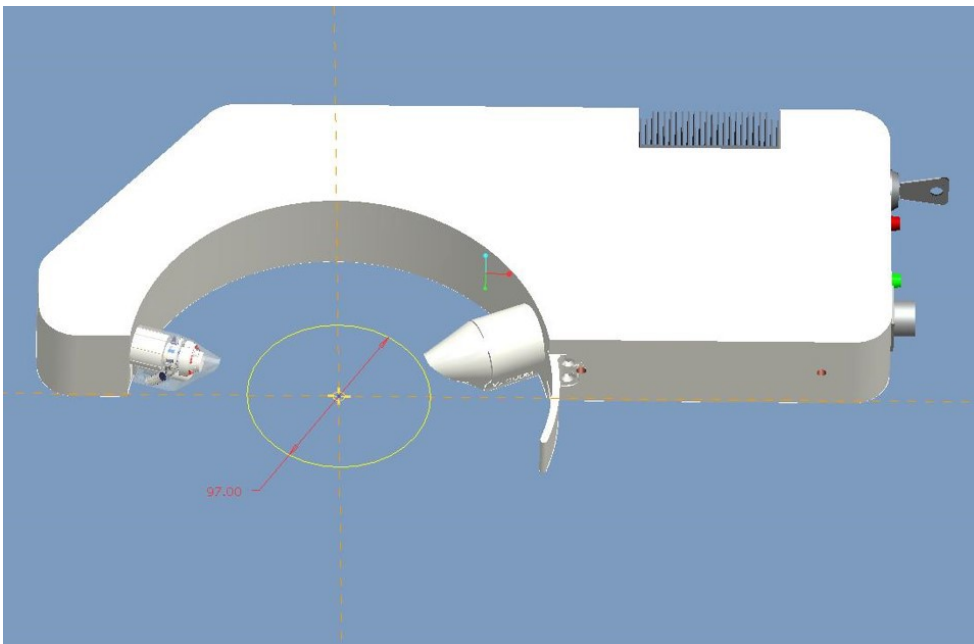


Figure 7.8: Schematic showing the TK2-PDI working distance with purge hoods.

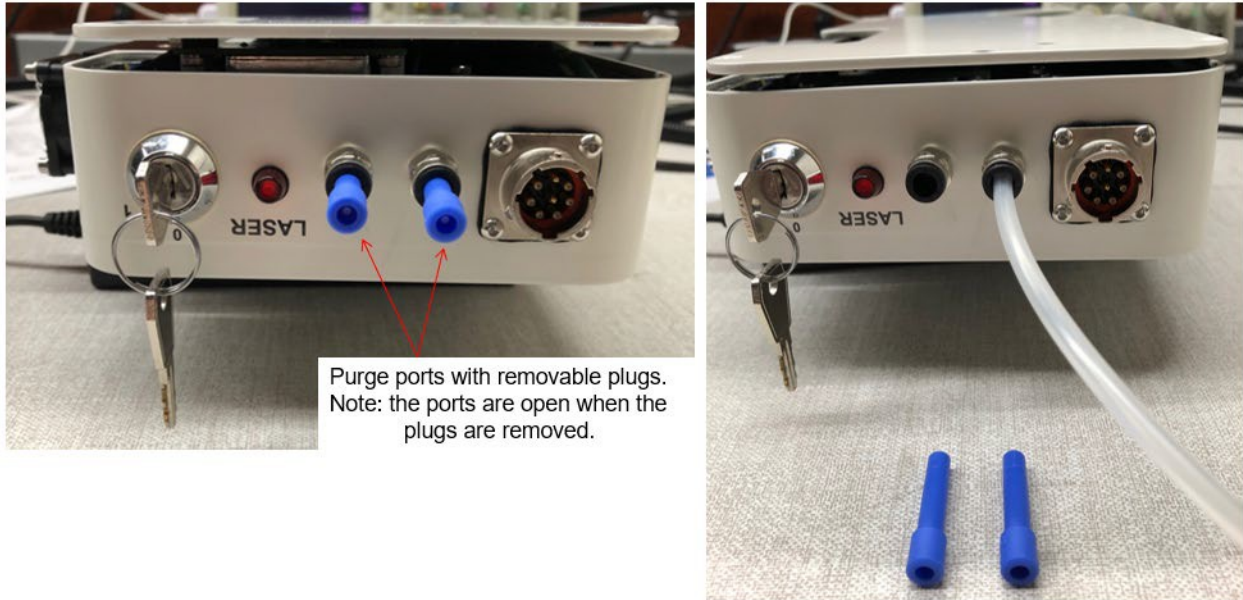
### ***Purge Air for TK body***

To prevent any moisture from entering, or condensation forming inside, the TK optical head, it is recommended that purge air be supplied using the available ports. Purge air should be clean dry air or bottled nitrogen.

The purge ports are push-to-connect designed for 6mm OD tubing.

Update: 9-Aug-19

Plugs are removed. Clean dry air at low pressure 10psi (0.07Mpa) max is supplied into one port. The other port is left open as an exhaust for the purge air – to prevent any excessive pressure build-up in the TK head.



### ***Purge Hoods/Beam Shields***

The TK-PDI is supplied with hoods that protect the windows from droplets, provide anti-fogging, and protect the light paths in cases of high number density sprays. The purge hoods require both pressurized air and vacuum, and they operate on low air pressure (5-10 psi) and low flow rate. Each hood attaches to the housing with a single M3 cap head screw.

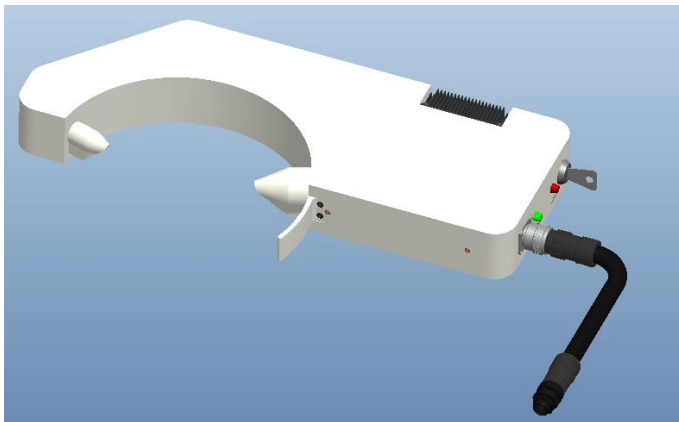


Figure 7.9: Beam shield / purge hoods installed on a TK2.

The design goal is that no air will exit the purge hood and affect the spray flow, but droplets will be prevented from entering the hoods and reaching the windows.

In most cases, the hoods alone are adequate to shield the beams and protect the windows from droplet accumulation. When this is not the case, the hoods are designed to work with both purge air and vacuum. Figures 7.10 and 7.11 show the external and internal construction of the hoods. There is a plenum for purge air that can be supplied via the PURGE port on the hood. Clean Dry Air (CDA) from a compressor or pressure cylinder source, or nitrogen, is required (not supplied by Artium). Artium supplies a pressure regulator and tubing.

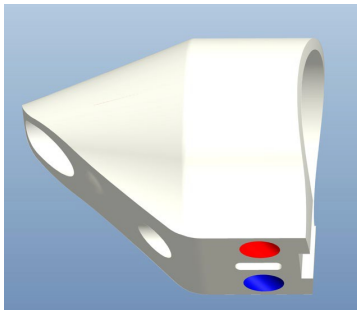


Figure 7.10: Purge hood external construction.



Figure 7.11: Purge hood internal construction.

The air enters the hood through radial ports along the inner circumference of the hood. This will create a slight positive pressure relative to the test flow and aid in keeping small droplets out of the hood and moisture from condensing on the TK windows. Some of this purge air will exit the hood through the open end and enter the test flow. It is important that this air not adversely affect the external flow under test. Only the minimum amount of purge air (a few psi pressure) should be used, and tests should be run to confirm that the test flow is not affected by the purge.

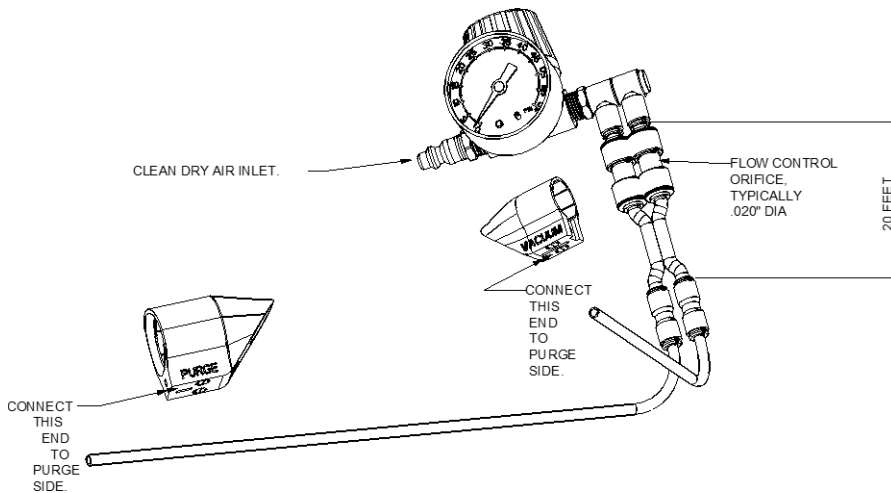


Figure 7.12: Purge hood plumbing supplied by Artium.

In cases where purge air is a necessity and there is the possibility that the air exiting the hood is affecting the external test flow, there is a separate plenum from which air can be drawn out of the hood. That port is labeled VACUUM. Artium does not supply plumbing for this feature. The vacuum plenum will draw air in through radial ports along the inner circumference of the hood. The purge and vacuum flowrates must be balanced so the net flow to the hood is zero. Too much vacuum can also adversely affect the external test flow.

## Chapter 8

### *Software Set-up*

#### **PDI-100 Device Setup Parameters**

**Before starting**, ensure that the software is set up for the correct instrument configuration. In the upper right hand corner of the AIMS screen, the Doppler Analysis box needs to show the appropriate instrument. In this case, it should be 1D PDI. If this setting is changed, you will be asked to re-start AIMS so the appropriate database is selected.

In this section, the setup parameters for the system processing electronics and software are described in detail. Although the instrument has a unique automated setup feature (U.S. Patent 7,788,067, EPO/AT537425T), it is important to know something about the meaning and function of each of these parameters so the user has a better understanding of the system operation. The function of these parameters is also needed in order to make intelligent judgments if manual setup is required. Manual setup may be needed in special cases when the signal-to-noise ratio is low or in very challenging measurement environments. The setup parameters are accessible by: using the **F4** function key, by selecting **Acquisition->Show Device Controls...** **simply clicking the mouse on the Device Controls icon on the top menu bar** of the AIMS software menu.

The parameters in the various tabs are described below.

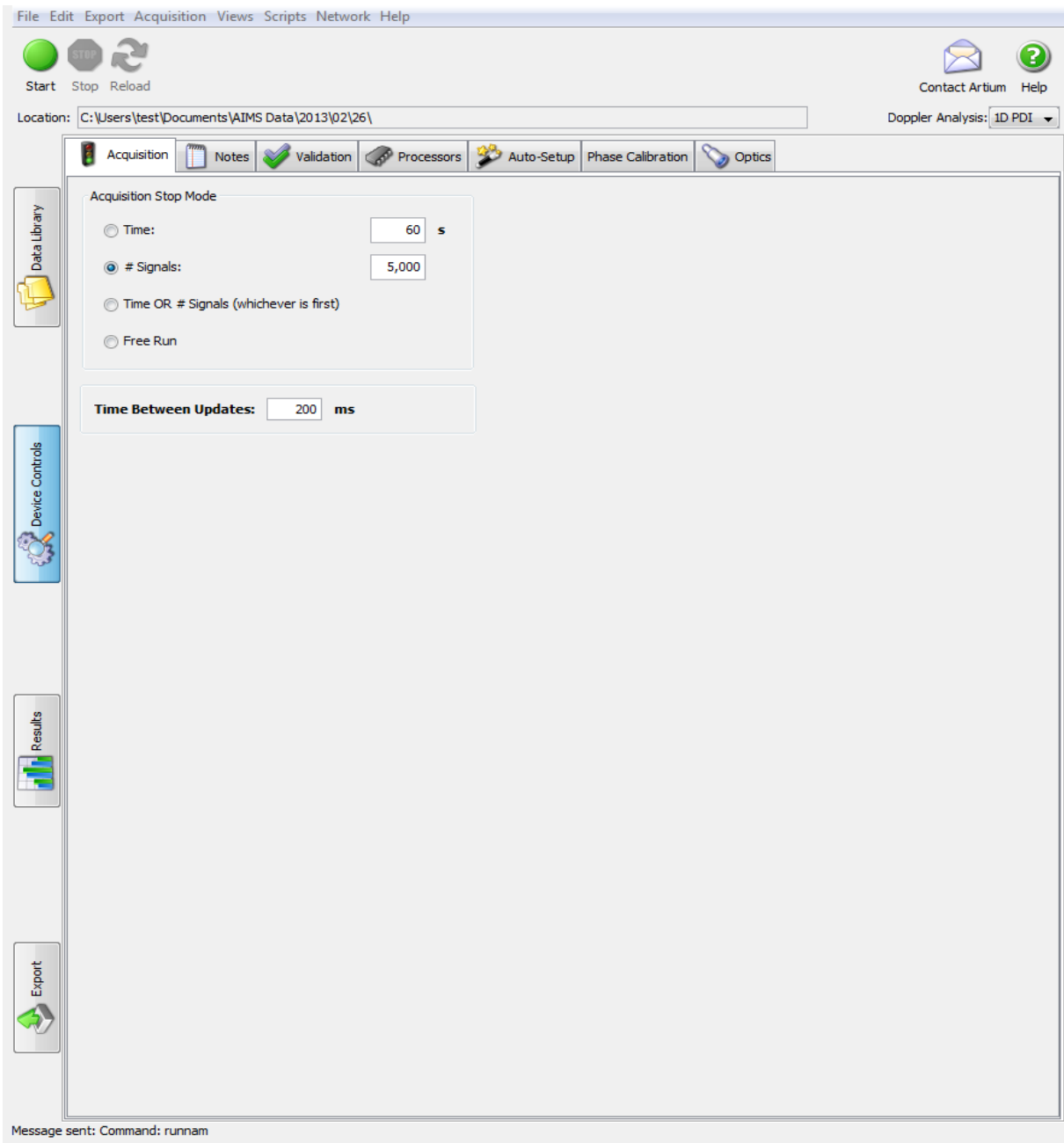


Figure 8.1: Acquisition Tab.

Acquisition	
Acquisition Stop Mode	Data acquisition shown in figure 8.1 may be controlled with three possible commands, Time, # Signals, and Free Run.
Time	This selection is used to set the total time (in seconds) for data acquisition. Acquisition will continue for this elapsed time and then stop irrespective of the number of samples collected.
# Signals	This selection allows the number of samples to be collected during

	<p>acquisition (before signal validation). This number is the sum of the measurements for all channels if a two or three velocity component system is used. Typical values are from 5,000 to 10,000 droplet measurements. Good statistical representation of the largest drops in the distribution requires a large number of measurements to be made.</p>
Free Run	<p>When this button is activated and data acquisition is started, the system will continue to take data until the stop button is pressed. This allows the user to observe the histograms of the size and velocity distributions and make a judgment as to when an adequate number of samples have been acquired. It also allows recording of data over extended periods of time when, for example, the spray is changing in time (for example, in-cloud measurements are being made with unpredictable arrivals of the droplets).</p>
Time between Updates	<p>The screens displaying the data will update at the time set on the field in seconds. A setting of zero is a default which means that the software will establish the screen update rate. Values of 0.3 to 0.5 are typical.</p> <p><b>WARNING:</b> Setting a value that is too small will significantly slow the processing.</p>
Notes	<p>This page is provided so that notes on the experimental setup, information on the experimental conditions and other information that are needed to describe the data acquisition conditions. The information is saved with each data file.</p>



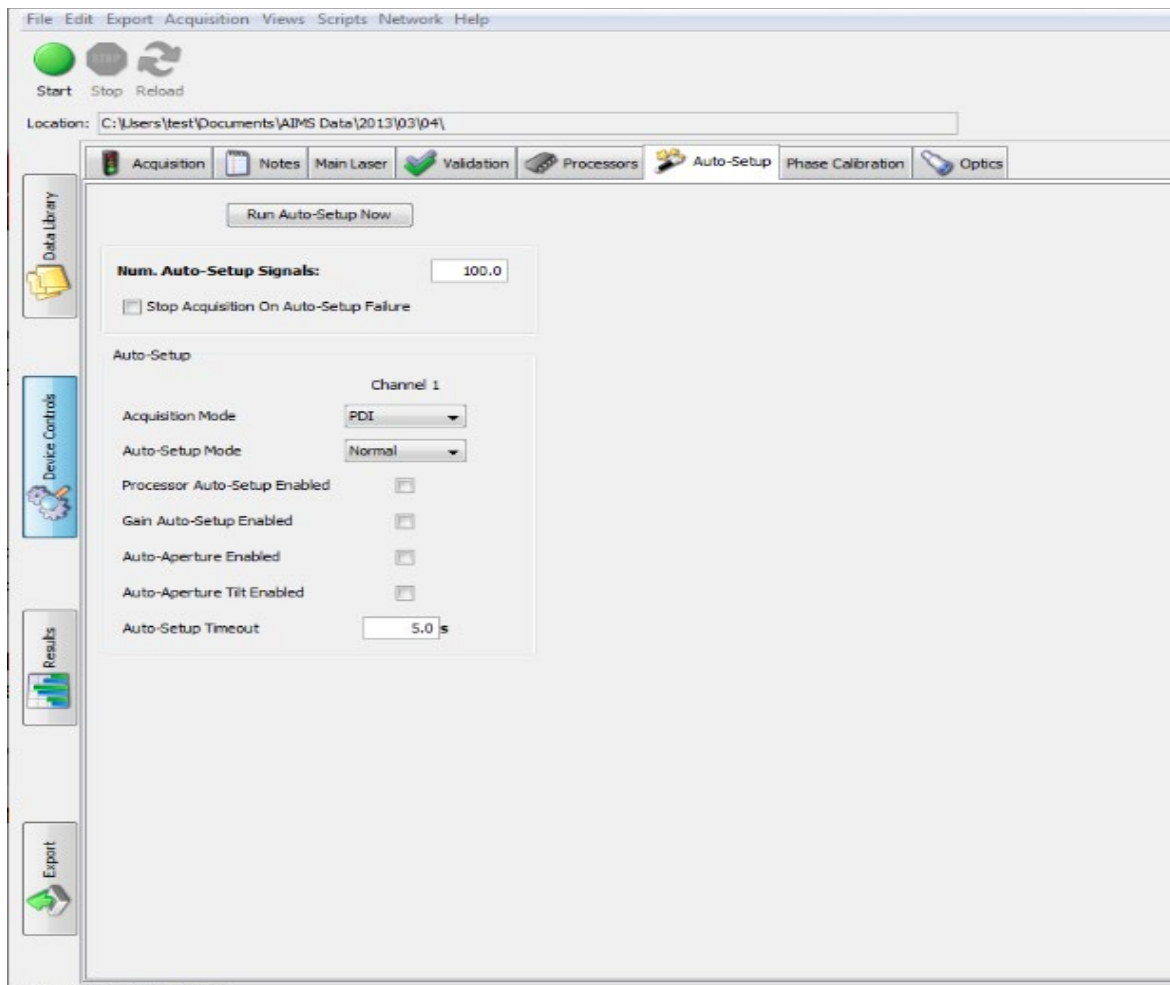


Figure 8.2: Auto-Setup Tab.

Auto-Setup	This tab allows the user to set up the instrument in either automatic or manual setup modes for channels 1, 2, and 3 by clicking in the box to set or remove a check mark. The check mark indicates Auto-setup is active.
Num. Auto-Setup Signals	In auto setup mode, figure 8.2, the instrument will use a set number of signals to measure the flow conditions and use that information to establish the optimum settings for the signal processor. This field controls the number of signals (per channel) that the auto-setup routines will use for the auto-setup of processor parameters. Typically, a value between 500 and 1000 signals is appropriate. At typical data rates of 2,000 to 10,000 samples per second, acquiring a thousand samples will only require a fraction of a second. Manual setup typically takes longer since the procedure is to set the instrument parameters, test the result, and possibly repeat the procedure until a suitable setup is attained.
Run Auto Set up Now	This command box allows the user to test the instrument and quickly set up the processor to the appropriate settings using the auto set up logic. Clicking on this box will command the instrument to take a fixed number of signals and determine the best setup for the signal processor, given the spray conditions at hand. This requires that signals are present produced by spray droplets passing the sample

	volume.
Mode	This selection allows one to indicate whether the instrument will be operated as a PDI (measuring size and velocity) or an LDV instrument (measures only velocity) which then affects the Auto-Setup functionality.
Processor Auto-Setup Enabled	Clicking the Box sets a check mark indicating the Auto-Setup is on for the respective channels. In general, these buttons can be left in the on position (check mark in the box). In some conditions the signal-to-noise ratio may not be adequate or due to other complications, it may be necessary to turn the Auto Setup to off by clicking on the box to remove the check mark and set the instrument up manually. This is the exception rather than the rule.
Gain Auto-Setup Enabled	Clicking the box for this function sets a check mark indicating that the automatic signal detector gain is operating. In order to get sufficient data to set the PMT gain, several thousand drops may need to be measured. Once again, at data rates of 1,000 to 10,000 per second, this easily wins over manual gain setting strategies. Currently, we are evaluating and perfecting the automatic gain setting algorithms. Until we have finished refining this function, set the Gain on the optics page manually. This will be described later (Figure 8.7).

## Phase Calibration

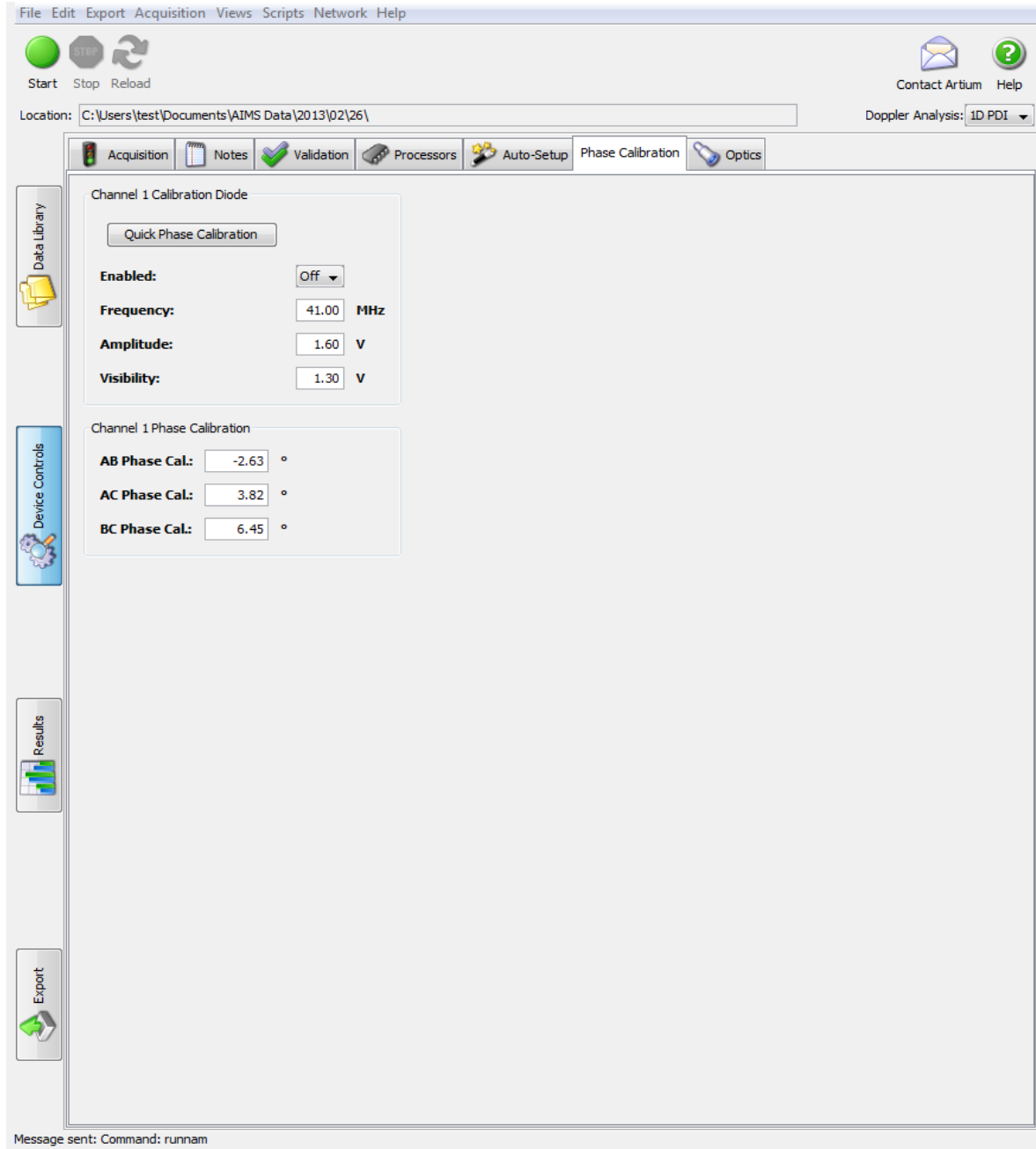


Figure 8.3: Phase Calibration Tab.

Calibration Diode	
Enabled On/Off	Periodically, the PDI instrument runs through a phase calibration procedure to ensure that there are no unexpected or uncompensated phase delays in the system. Because of the high signal frequencies that occur, small differences in the transit time of electrons through the electronic components can produce phase differences between the signals that might have a significant impact on the measurements. Since accurate particle size measurements depend heavily on the determination of phase differences between the photodetectors, it is critical

	<p>that these differences due to the electronics are canceled. Phase calibration, figure 8.3 has been incorporated to subtract out the phase differences that may occur due to the photodetector electronics, signal cable length differences and the signal processor. Because the differences in the phase are caused by different transit times and electronics, the measured phase shift will also depend on the signal frequency. Thus, the phase calibration must be conducted at or near the expected signal frequencies produced by the drops passing the sample volume.</p> <p><b>Notice:</b> When performing phase calibration, cover the receiver lens with the lens cover so that there are no actual signals interfering with the phase calibration signals. One may also turn off the spray or block the laser beams with the transmitter lens cap.</p> <p>The <b>Enabled On/Off</b> command turns on the calibration laser diode that generates an identical simulated optical Doppler signal to each of the photodetectors.</p> <p><b>NOTE:</b> Set the Amplitude to a value that produces signals with an amplitude (viewed on the Oscilloscope) of between 100 and 200 mV. The calibration signal also depends on the detector Gain setting. This value should be set with the spray on so that the actual signals are in range. This will ensure that the detector Gain does not affect the phase calibration. However, the phase is relatively insensitive to the Gain setting.</p> <p>The instrument measures any phase differences between the signals and sets compensation values so that the relative phase shifts are all zero. Although all of the detectors and preamplifiers have been designed to minimize electronic phase shifts, this final procedure insures that very precise and accurate phase measurements are being made.</p>
Frequency	<p>This command sets the signal frequency produced by the calibration laser diode and should be set to values close to the expected Doppler frequency of the actual signals produced by droplets plus the 40 MHz shift frequency (45 MHz on Ch 2, 80 MHz on Ch3). A value that is relatively close to the expected value is adequate.</p> <p>An estimate of the signal frequency may be obtained as follows. First, an estimate of the flow velocity is made or a sample measurement may be obtained with the instrument to get the velocity of the spray flow. Doppler signal frequency is given as:</p> $f_D = \frac{\bar{V}}{\delta}$ <p>where V is the mean velocity and <math>\delta</math> is the fringe spacing given on the transmitter setup page. The signal frequency is</p>

	$f_r = \frac{\bar{V}}{\delta} + f_s$ <p>where <math>f_s</math> is the shift frequency of normally 40 MHz, and <math>f_r</math> is the approximate value that should be set in the frequency field (in MHz).</p>
Amplitude	<p>The <i>Amplitude</i> command is used to set signal amplitude of the simulated signal. Generally, a value between 1 and 3 produces the appropriate signal level. Simulated signals should be observed on an oscilloscope to ensure that they are approximately equal to the mid-amplitude range of the actual signals. Observing the Raw signals using an oscilloscope connected to the RAW signal monitors on the ASA processors, the signal amplitudes should be between 100 and 500 mV.</p>
Visibility	<p>The <i>Visibility</i> command adjusts the degree of modulation on the Raw signal monitor at the back of the ASA signal processor (signal directly from the photodetector which has not been high pass filtered). The appropriate values for the setting lie in the range of 1 and 3. A value should be set so that the modulation depth is slightly less than the minimum value of the signal or stated another way; the bottoms of the oscillations do not fall to zero voltage or negative when observed on the oscilloscope.</p>
Quick Phase Calibration	<p>Quick Phase Calibration command may be used to set up the calibration automatically. In most cases, this approach is the fast efficient way to calibrate the detectors. <b>Remember to set the Frequency</b> to approximately the expected signal frequency for the measurements. Using this command, the instrument measures a set number of signals and determines the phase shift for each of the detectors and automatically sets these values into the AB, AC and BC Phase Cal boxes under the heading <b>Channel 1 Phase Calibration</b>. Using this method, the phase Cal data are not observed. If one wishes to observe the phase Cal results, the manual phase Cal approach may be used. With this approach, the laser diode is activated by setting enabled to <b>On</b>. Under the AIMS main data acquisition page, select Views -&gt; PDI -&gt; Misc. -&gt; Phase Calibration. This page will show the phase shift for each pair of detectors (AB, AC, and BC). Click the Green button on the software user page to acquire data and then take the mean phase values and enter them with the <b>OPPOSITE SIGN</b> into the boxes for AB Phase Cal., AC Phase Cal., and BC Phase Cal. It is advisable to take several trials to ensure that the phase cal signal is producing stable results (mean not varying more than a few degrees). If the mean value is varying, ensure that the Phase Cal signals A, B, and C have amplitudes that do not differ by more than +/-30%.</p> <p><b>WARNING:</b> Be sure to <b>turn off</b> the Cal diode when using the manual calibration procedure. Quick Phase Calibration automatically turns off the calibration diode.</p>

### Validation

This tab shown on figure 8.4 allows the user to set the validation criteria for the instrument. Our new PDI instruments have a number of important validation criteria that each signal must pass before it is accepted as a valid measurement.

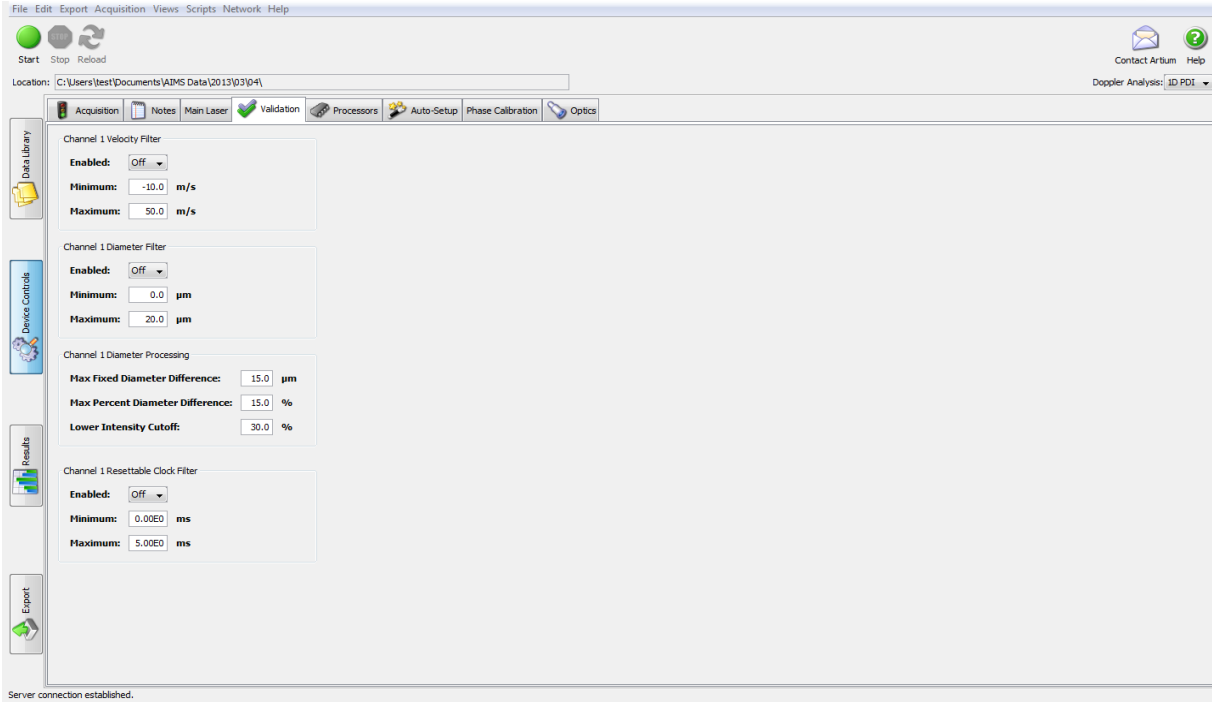


Figure 8.4: Validation Tab.

Channel 1 Velocity Filter	
Enabled	By turning this function to On, it sets the upper and lower limits of the velocity values that can be measured. It can be used to truncate the velocity measurements or to eliminate any potential spurious readings (“outliers”) on the signal-to-noise ratio of the incoming signals as low. When the velocity filter is enabled, velocity readings less than or greater than the minimum and maximum values will not be recorded or incorporated into the computations of the mean and RMS velocity values. This constraint is generally not needed.
Diameter Filter	When the Diameter Filter function is enabled by turning it to On, it serves to limit the minimum and maximum drop sizes that will be measured at this setting. The function can be used to limit measurements outside of the range of interest.
Diameter Processing	
Max Fixed Diameter Difference	This is the maximum difference in the measured drop diameter for detectors AB, AC, and BC. This value is typically set to a fixed difference of from 10 to 15 um and 15% of the measured drop size. Recall that the instrument measures a drop size for each of the three pairs of detectors. Detectors AC produce the greatest sensitivity (change in phase relative to droplet diameter) followed by BC and then AB. Artium Technologies uses a unique approach using all three detectors to produce 3 drop size measurements for each droplet. These measurements are compared to the weighted mean value of the three measurements and if the difference of the size measured by any pair of detectors falls outside of the acceptable uncertainty band, the measurement is rejected. This validation scheme is very effective in eliminating faulty measurements from the measured drop size distribution.

Max Percent Diameter Difference	This is the maximum percent difference in the measured drop diameter for detectors AB, AC, and BC. If a small, fixed diameter difference is used for the small drops that fixed difference may be too small for the large end of the size distribution.
Max Phase Pair Difference	This is the maximum acceptable difference in the phase shift over the duration of the signal. By testing the phase shift over the signal duration, any changes in phase due to mixed light scattering components (reflection and refraction) which can cause significant measurement error can be detected and the sample will be rejected (U.S. Patent 7,788,067, EPO/AT537425T). This approach is used to ensure that the wrong light scattering component has not contaminated the information on the signal which could lead to significant sizing errors.

### Processors

The ASA Processors tab shown on figure 8.5 controls the signal processor functions and allows manual setup of the system, if necessary. Each of the signal processor functions are defined in this section and some advice on setting up the system are provided. In general, for normal spray measurements, the auto setup mode should be used. Highly experienced users may want to try other settings and this page allows this procedure.

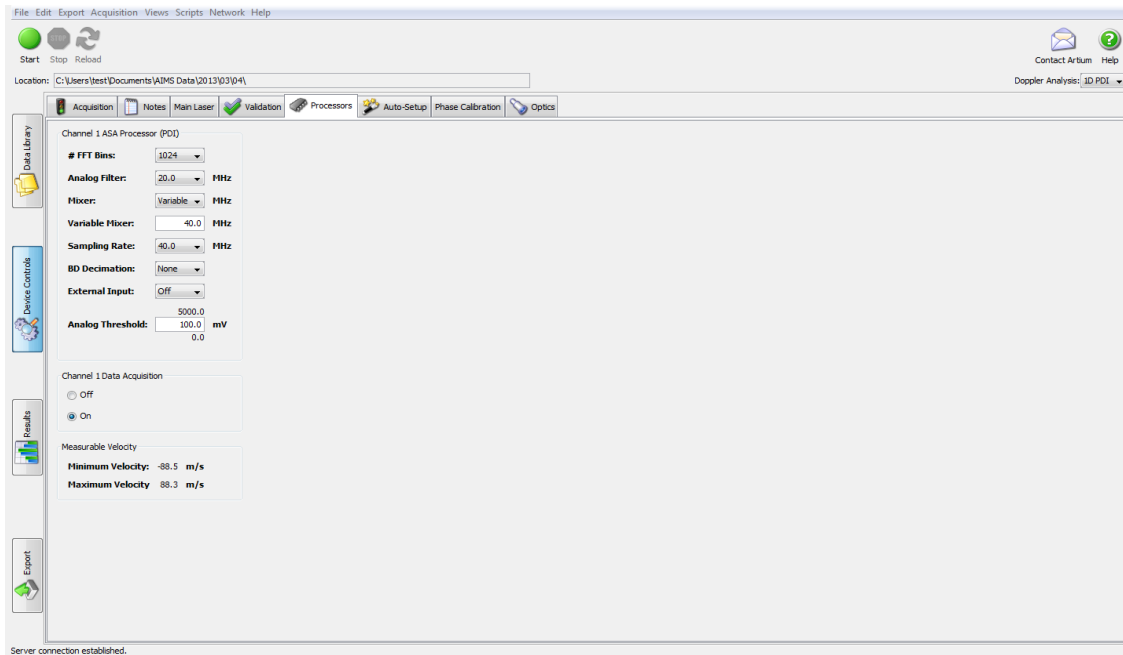


Figure 8.5: ASA Processor Tab.

Channel 1 ASA Processor	
# FFT Bins:	The calculations of the Fourier transform are normally completed using 1024 frequencies which is also the maximum number of samples collected over the signal duration for signals that are long enough. It is also possible to compute the FFT with more frequencies to obtain a higher resolution on the frequency and phase. In general, a value greater than 1024 is not necessary but values of 2048, 4096, and 8192 may be used in very special

	cases.
Analog Filter	The analog filter serves two purposes; it helps to reduce the noise on the signal and removes the sum frequency produced by the frequency mixer. When using a mixer, a local oscillator frequency is mixed with the Doppler signal plus frequency shift. The mixer produces the sum and difference frequencies of these signals. The sum frequency needs to be removed. This is described in detail in the following paragraphs.

The signal consists of a high frequency Doppler component superimposed upon the low-frequency Gaussian pedestal component. The signal frequency is directly related to the velocity of the particle through the relationship:	$v = f_D \delta$
The fringe spacing of the interference pattern is determined by the wavelength of the laser beam and the beam intersection angle and is given by the following expression:	$\delta = \frac{\lambda}{2 \sin(\gamma / 2)}$
The raw signal produced by the photodetectors and received by the signal processor is a combination of the Doppler frequency and the shift frequency, $f_s$ produced by the presence of a Bragg cell. The signal frequency is given as:	$f_r = f_D + f_s$
The raw signal first passes through a fixed frequency high pass filter set to remove the pedestal component of the Doppler burst signal and any low-frequency noise. The signal is then combined with the mixer frequency, $f_m$ which produces a signal as follows:	$f = (f_r - f_m) + (f_r + f_m)$
This resulting signal is passed through the low pass or Analog filter to eliminate the high frequency components including the sum frequency, $(f_r + f_m)$ , from the mixer and any high-frequency noise. The remaining frequency is given as:	$f_t = f_r - f_m$

A low pass filter must be set just above the highest frequency,  $f_i$  present in the signal with sufficient margin to ensure that the high-frequency excursions in the flow field pass the filter. Using the above expressions along with the knowledge of the highest expected velocity, a rough estimate of the maximum frequency can be made. If the setting is too low, it will be evident from the measured velocity distribution in the first measurement trial. When in manual mode, a few iterations may be necessary to optimize the analog filter setting.

Mixer	The mixer frequency is the value used to drive the electronics mixer that forms the sum and difference of the resultant frequency. This frequency value is set to obtain a reduced frequency in the desired range for processing as shown in the above expressions. There are fixed mixer frequency settings of 80, 40, 38, 36, and 20 MHz. There is also a variable mixer setting which allows any value in the range of 5 to 45MHz to be set. Setting the proper mixer frequency requires some experience and is best left to the automatic setup. In manual mode the mixer may be set to minimize the signal frequency and allow a low analog filter setting which also serves to filter the noise. Care must be taken to not set
-------	--



	<p>the Mixer so that some frequencies in the range of droplet velocities measured do not fall at zero frequency. The phase shift of zero frequency signals is undefined. Also, if the analog filters are set too low, filtered noise may appear to be sinusoidal in nature over short periods of time. This can lead to false detections by the signal burst detection system. After processing the signal using the Fourier transform, the signals will be rejected. However, too many false detections could slow the data acquisition rate or interfere with the detection of real signals.</p>
Variable Mixer	<p>The variable mixer field allows input of any mixer frequency in the range of 5 to 45MHz. The variable mixer capability is very useful when working at low signal frequencies where positioning the frequency in the right range will allow optimization of the processing functions. Once again, the auto setup algorithm does a very good job of picking the right combination of mixer of value, analog filter, and sampling frequency to optimize the signal processing.</p>
Sampling Rate	<p>The sampling rate refers to the frequency at which analog to digital conversions are performed. The processor has the capability of sampling the Doppler burst signals at up to 160 MHz for both the real and imaginary components of the signal. This is an equivalent sampling frequency of 320 MHz. The sampling frequency also needs to be set according to the resultant signal frequency, <math>f_r</math>. For laser Doppler velocimetry applications where only the frequency of the signal is of interest, the sampling frequency must be greater than twice the resultant signal frequency, <math>f_r</math>. When measuring the phase shift between signals, a higher sampling frequency is preferred since it provides better resolution on the phase measurements. With Quadrature Mixing (Mixer) used in our systems, clearly almost any frequency can be set for signal processing. However, the signal bandwidth and duration are critical parameters that need to be considered when selecting the sampling frequency. If the velocity fluctuations are large, the sampling frequency must be set to meet the Nyquist criterion for the highest frequency (sampling frequency greater than twice the signal frequency). A minimum number of samples need to be acquired over the period or duration of the signal. For example, the Gate signal or signal length can be observed on an oscilloscope to estimate the minimum signal duration. Because of the complexities in setting the appropriate sampling frequency, it is best to use the Auto-Setup which optimizes the selection of the sampling frequency and other processing parameters.</p>
BD Decimation	<p>If the sampling frequency is greater than twice the analog filter setting, it is possible that the digital burst detection system will trigger too frequently on noise. This occurs because the higher frequency noise in the signal has been filtered leaving low-</p>

	<p>frequency noise. Low-frequency filtered noise over short durations may appear to be coherent or periodic and therefore the burst detector could recognize it as a signal. To avoid this problem while using higher sampling rates, the sampling rate for the burst detection system is reduced by the factor in the BD Decimation field (None, 2, 4). The automatic setup will select the appropriate value. However, if manual setup is used, the rule of thumb is to have the sampling rate divided by the BD decimation equal to twice the analog filter value.</p>
External Input	<p>The setting alerts the system to the presence of some other device that inputs information such as temperature, pressure, etc. that will be measured at the same time as a particle size and velocity are measured. This information is attached to the size and lost information on the function is turned on.</p>
Analog Threshold	<p>There are two signal detection systems in the ASA signal processor; a digital and analog detection system. The analog threshold allows setting a voltage threshold level at a specific value for signal detection. This is necessary if, for example, there is a low level coherent noise signal in the background. In this case the digital burst detection system will detect a signal when a Doppler signal is not present. Setting the analog voltage threshold level above this coherent background noise level will prevent the processor from detecting the background. Analog Threshold sets the start detection level. These values do not need to be set but in general, are set to 100 mV which represents a level of about 1 to 2 mV on the Raw Signals. Typically, values of from 100 mV to 300 mV are used. It is not generally necessary to adjust this value.</p>
Channel 1 Data Acquisition	<p>This software switch activates this channel. If the switch is set to Off, the channel will not show any data.</p>

## Optics

This page shown in figure 8.6 provides information on the optical setup of the PDI instrument and allows setting those optical parameters that may need to be changed to adjust the system for the prevailing spray conditions.

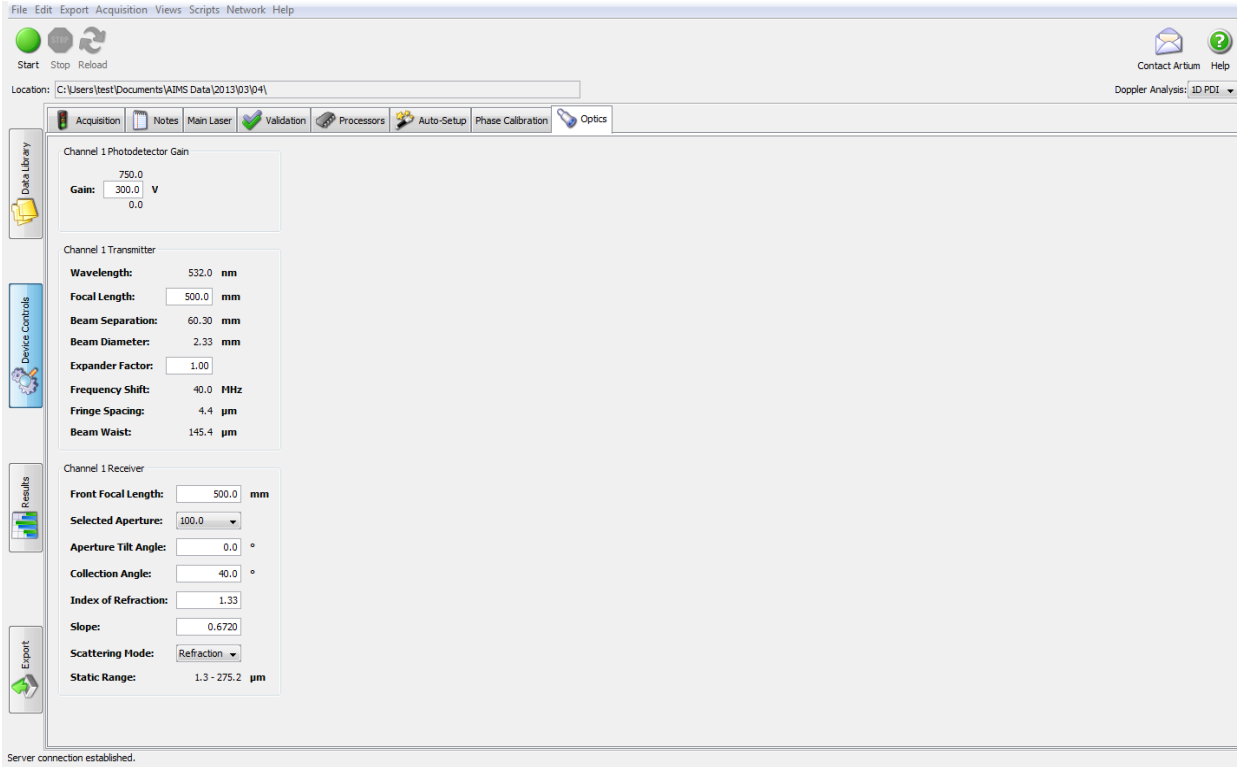


Figure 8.6: Optics Tab.

### Photodetector Gain

<p>Channel 1 Photodetector Gain</p>	<p>This allows setting the photodetector gain or high voltage to an appropriate value that depends upon the drop size distribution to be measured, the focal lengths of the receiver and transmitter, and other factors. The photodetectors or photomultiplier tubes convert the scattered light imaged onto them into electrical signals which are then processed to produce the velocity and size information.</p> <p>The most reliable method for setting the detector Gain is to use the plot of signal amplitude versus drop diameter under Results&gt; Views&gt; PDI&gt; Misc&gt; Ch1 Peak Intensity vs Diameter to obtain a plot of the signal amplitudes versus drop size, figure 8.7. Take a trial reading. If the Peak amplitudes for the largest drops are below about 1000 mV (red line), increase the Gain by 50 volts. Repeat until the largest drops have values near the red line. Some readings can be above the red line. Ensure that the minimum values are at or just above the “0” Peak voltage level.</p>
<p>Creating a New Export Template</p>	<p>Right-click on any screen item (graph, table, value, etc.) to open the context menu: Select Add To Export Template-&gt;New Export Template... In the Save Export</p>
<p>Template Dialog</p>	<p>Enter a name for the export template and click Save (figure 8.11). This will create the export template with the selected screen item as the first exported value.</p>

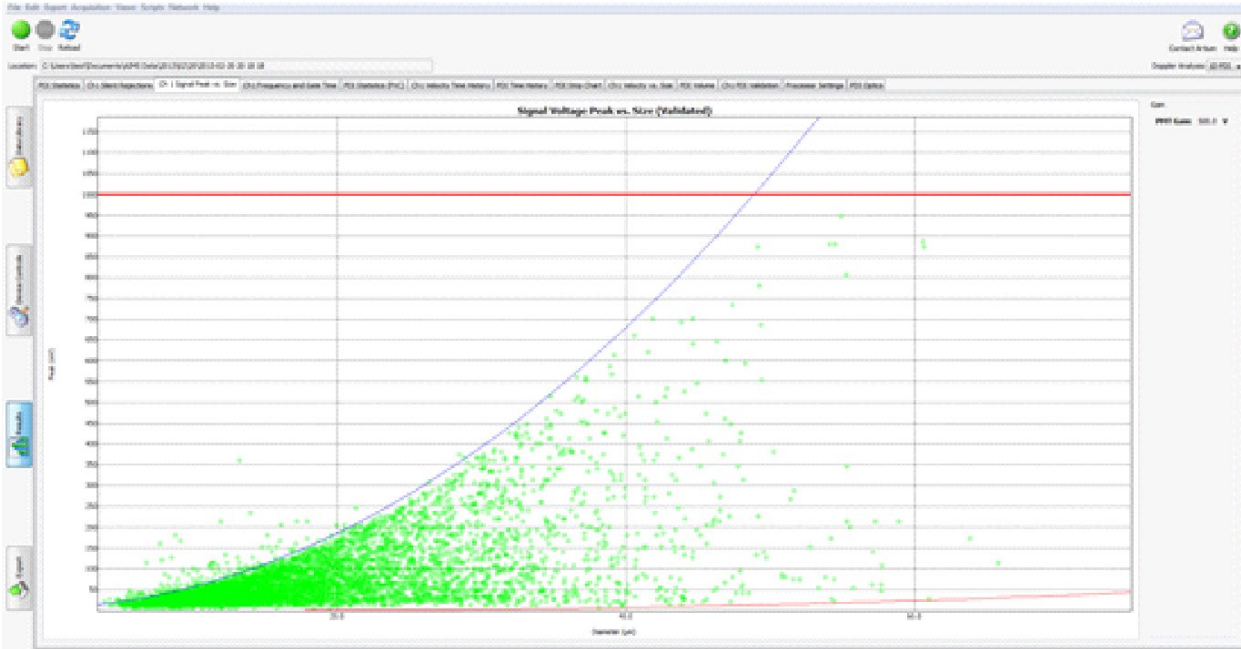


Figure 8.7: Plot of the signal intensity or peak voltage versus the droplet diameter. Since droplets scatter light in proportion to their diameter squared, the curve fit is a parabola.

## Chapter 9: Data Analysis

### Test Data Analysis

After the PDI-100 MD hardware has been properly connected and the various software parameters have been properly set, data acquisition may be initiated by clicking on the green button in the software user interface page or pressing the F9 key. The following figures show the various data screens that can be viewed by selecting the appropriate tabs. These screens provide information on the drop size, velocity, mean values, and temporal information on the spray. A short description of the information on each screen is provided to aid the user in interpreting the data being acquired. By right clicking on any of the plots, the plotting parameters may be changed and the graph limits adjusted as desired.

### 1D-PDI Statistics

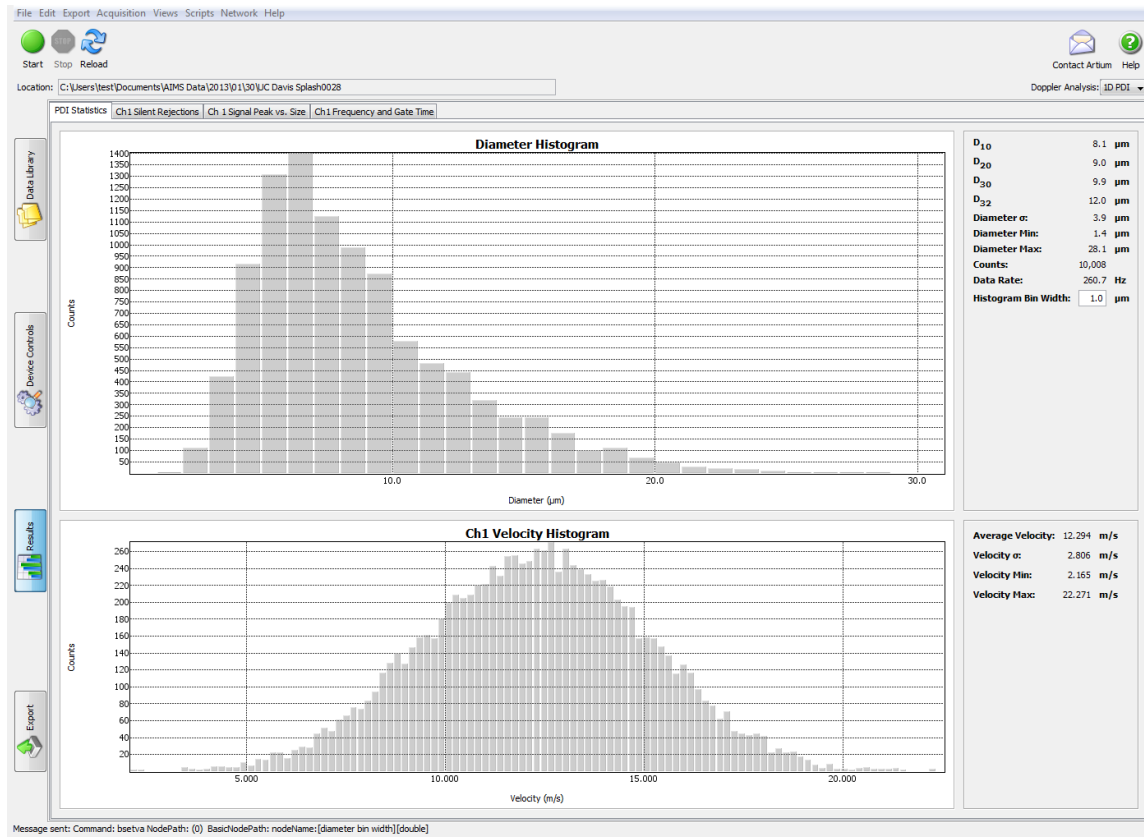


Figure 9.1: Diameter histogram and velocity histogram.

# 1D-PDI Statistics PVC

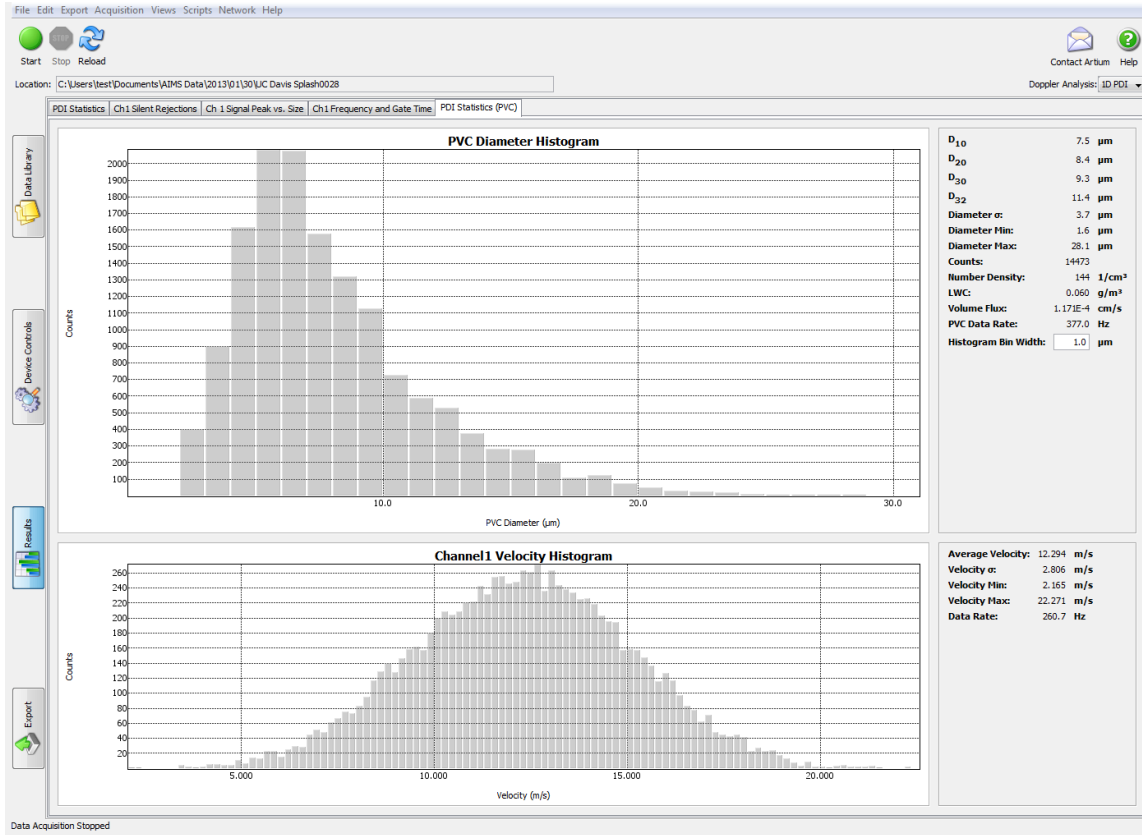


Figure 9.2: Probe volume corrected diameter histogram and velocity histogram.

Figure 9.2 is similar to Figure 9.1 except that the data have been corrected for the effect of varying sample volume on the drop size. Since smaller droplets have a smaller effective sample volume, the number in each size bin must be increased by a factor equal to the ratio of the sample volume for the largest drops to the sample volume for the drops in each size bin. This normalization approach compensates for the sample volume affect by increasing the number of drops in the smaller size bins. As noted from the mean values, especially D<sub>10</sub>, the mean size is decreased by the sample volume correction. It is important to note that the sample volume correction is necessary for an accurate measurement of the size distribution. This is the size distribution that should be reported.

## 1D-PDI Time History

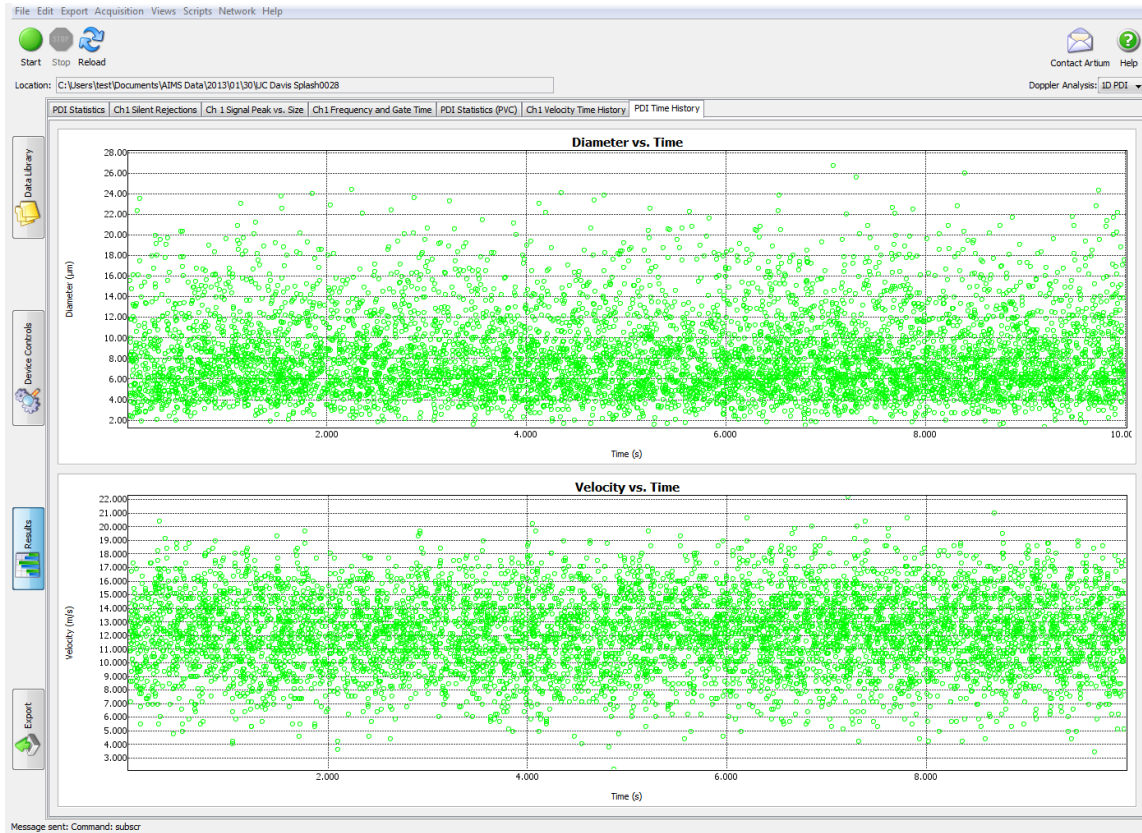


Figure 9.3: Time history plot of diameter and velocity.

## 1D PDI Strip Chart

Figure 9.4 also shows the diameter and velocity information as a function of time but displays it as a strip. This display is useful for viewing long time records over a short, elapsed time period to observe any time-dependent details in the spray.

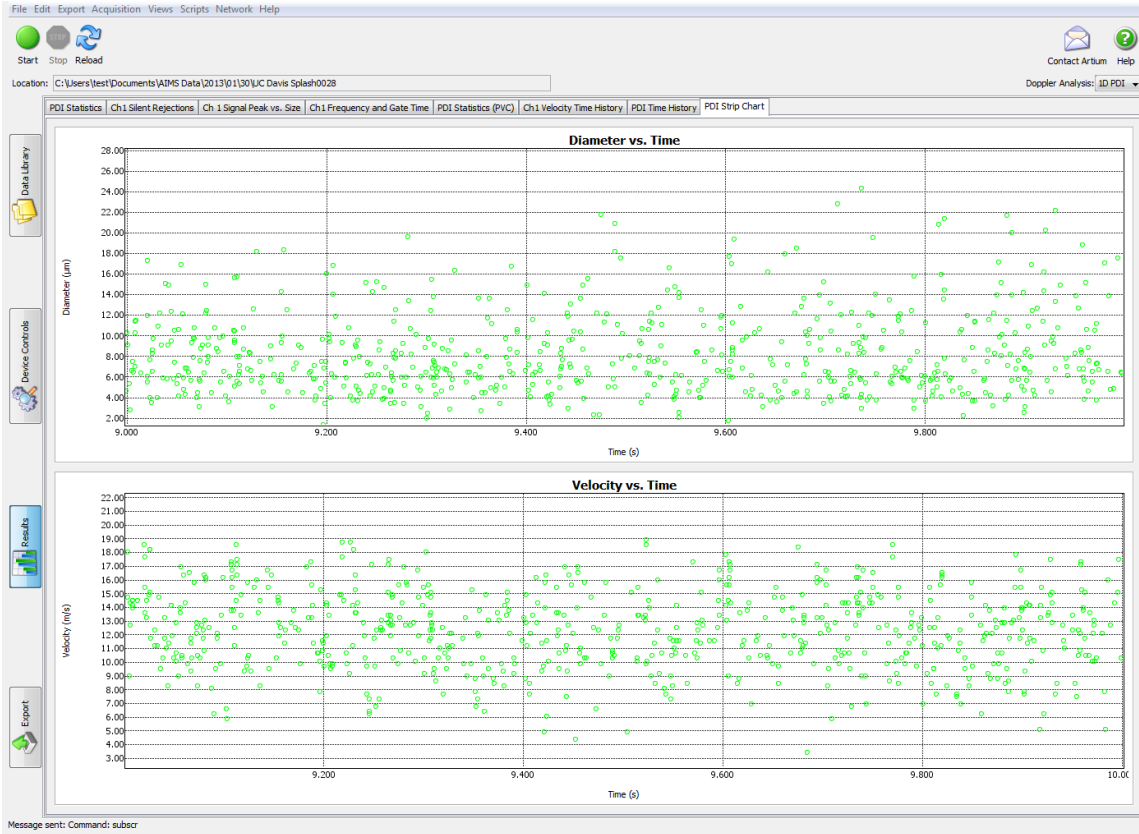


Figure 9.4: Strip chart plot of diameter and velocity.

### Velocity vs. Size

Figure 9.5 shows a very useful plot for observing the droplet dynamics. Each point on the graph is a single drop measurement of the drop and velocity. In this case, it is easy to see that the small drops have relaxed to the slower ambient flow velocity and that the larger drops have a higher velocity because of their greater initial momentum.

Since the PDI instrument responds to droplet flux, the relative velocity of the drops will affect the size distribution. To convert the size distribution to a concentration dependent distribution, the number of counts in each size bin needs to be normalized to remove the effect of the drop velocity for each size class. This needs to be done, for example, when the results are being compared to imaging techniques or to a line-of-sight ensemble light scatter detection method. The shape of this size versus velocity plot also helps to explain the shape of the size distribution described previously. Counts in the bins of the size histogram are affected by the relative velocities of the drops in the different size classes.



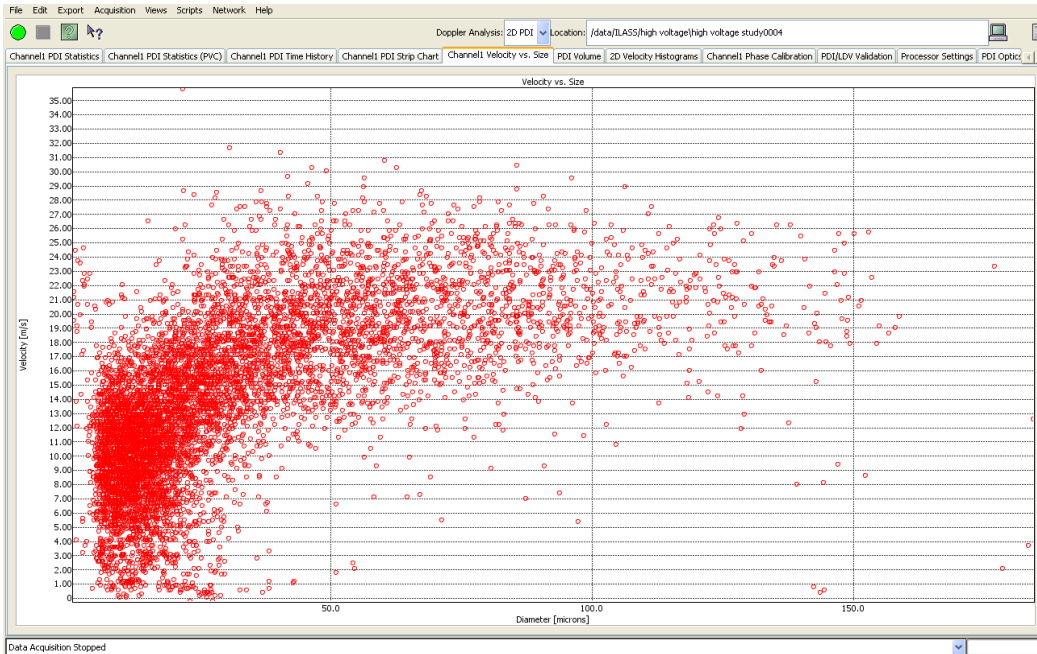
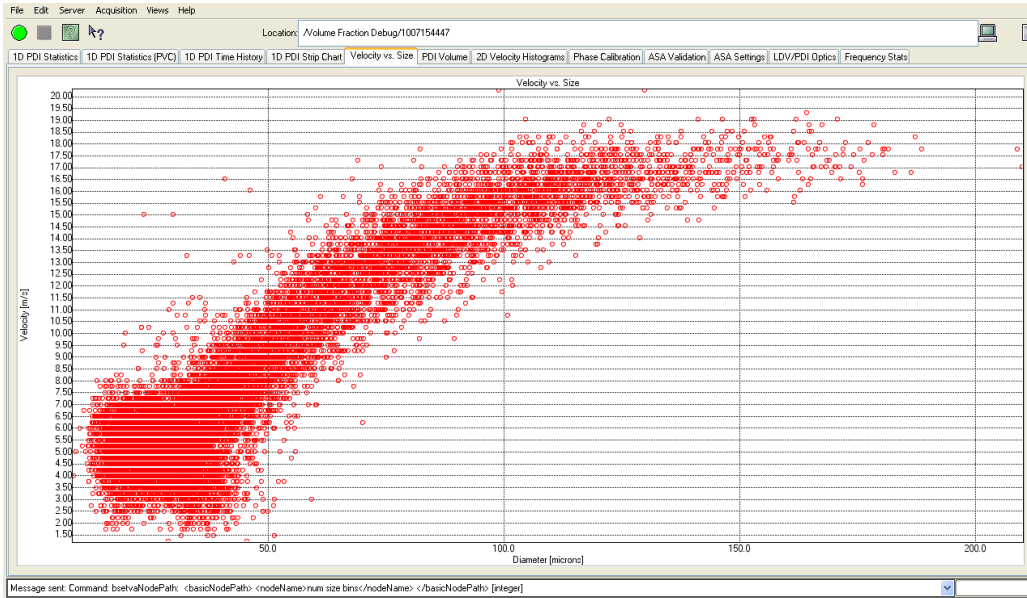


Figure 9.5: Examples of Velocity vs. Diameter plots.

## PDI Volume

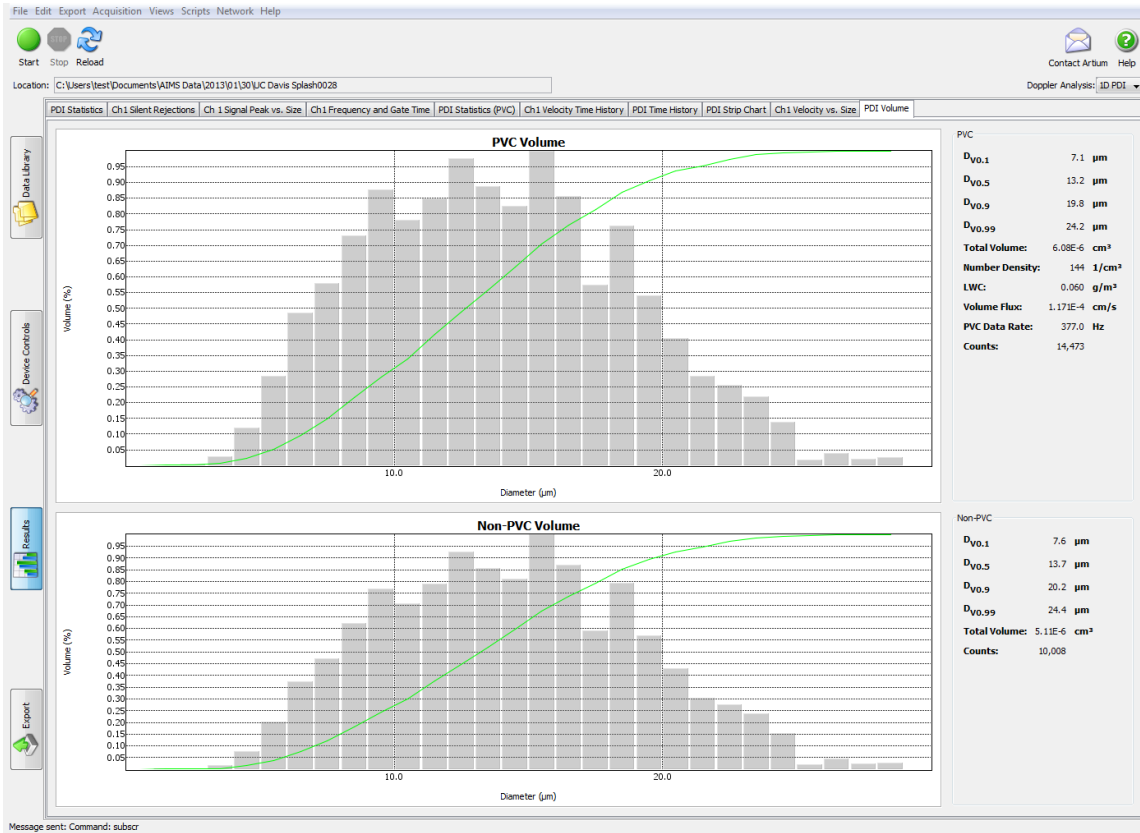


Figure 9.6 : Volume distribution (PVC and non-PVC).

Figure 9.6 shows the volume contribution for each size class of the spray drop size distribution. Also shown in the plot is a cumulative volume contribution for the various size classes. The 0.5 point on the plot is used to obtain the median volume diameter (MVD). The upper plot shows the size distribution that has been corrected for the probe volume affect (PVC) whereas the lower plot is the volumetric contribution for the uncorrected raw data (Non-PVC). The PVC corrected data is what should be used in reporting the measurements.

## ASA Validation

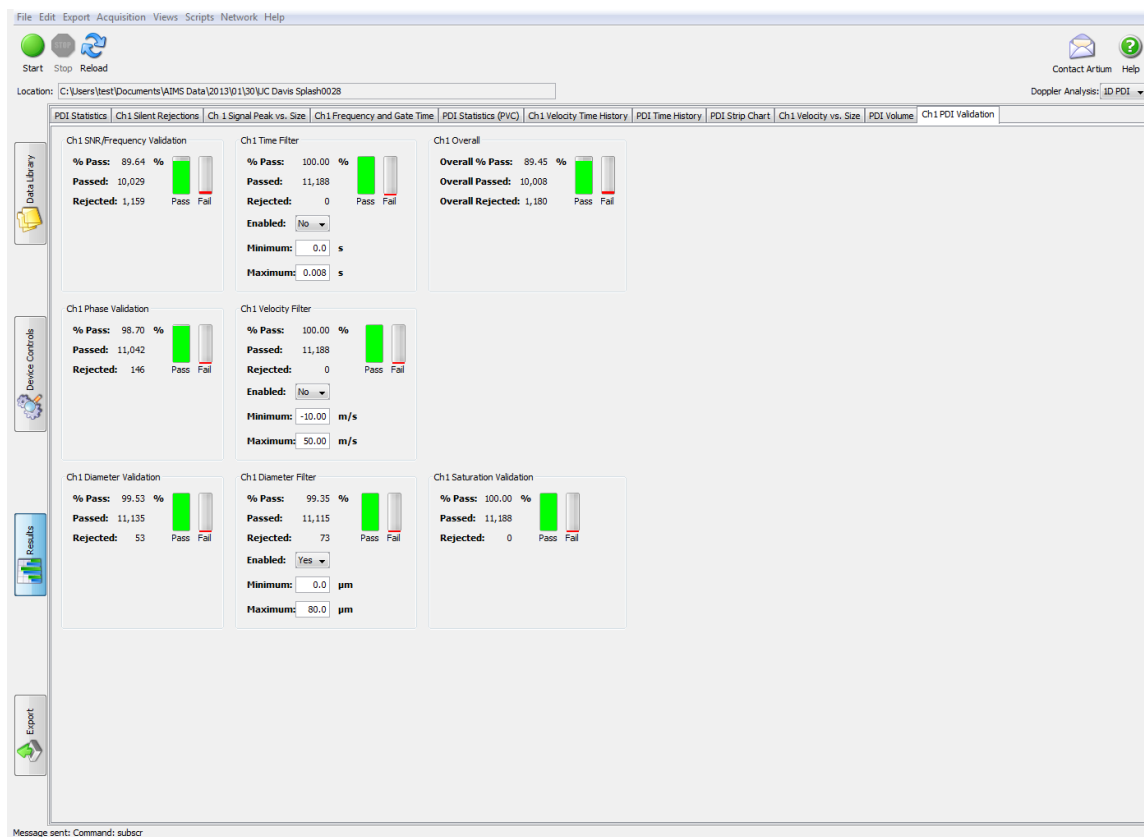


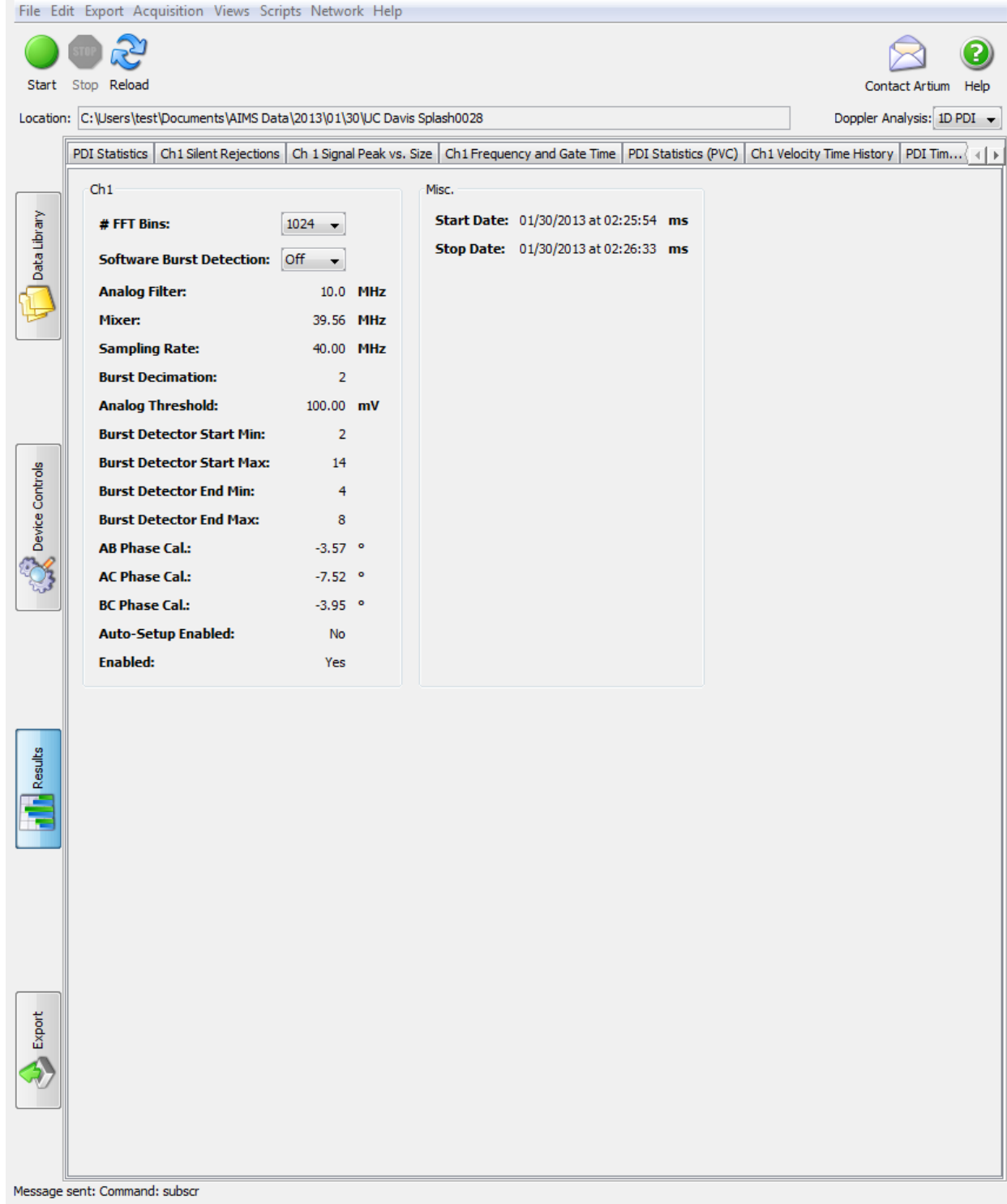
Figure 9.7: Channel 1 data validation results.

Figure 9.7 shows the screen that provides information on the percentages of attempted measurements that pass the various criteria before a measurement is accepted as a valid estimation of the drop size and velocity for Channel 1. The validation percentage provides an indication of the quality of the signals being detected but low validation rate does not necessarily mean that the instrument is making faulty measurements. Our proprietary digital Doppler signal detection method is programmed to detect signals based on their coherency (whether or not they have sinusoidal characteristics). Since we do not want to miss any droplets the detection is set to attempt measurements of even low amplitude, low SNR signals. The small drops will produce the weakest signals with low amplitude and low SNR but we do not want to bias the measurements by missing the small drops in the distribution. Furthermore, false signal detections will be discarded once the signals are processed with the full complex FFT and the remaining validation criteria have been applied. If the detection is set too conservatively, the validation will be very high but at the expense of missing the small drops.

Our innovative burst signal detection system has been designed to reliably detect even the smallest signals while minimizing false signal detection. Thus, the validation rates are usually high. However, in difficult sprays (dense sprays, sprays with very small drops but that are large in area, etc.) the validation rate may be expected to fall somewhat.

Each of the validation criteria have been described in the Device Control section under the Validation Tab. The rates shown here are in response to the criteria described in that section.

## ASA Settings



File Edit Export Acquisition Views Scripts Network Help

Start Stop Reload

Location: C:\Users\test\Documents\AIMS Data\2013\01\30\UC Davis Splash0028

Doppler Analysis: ID PDI

PDI Statistics Ch1 Silent Rejections Ch 1 Signal Peak vs. Size Ch1 Frequency and Gate Time PDI Statistics (PVC) Ch1 Velocity Time History PDI Tim...

**Ch1**

# FFT Bins:	1024
Software Burst Detection:	Off
Analog Filter:	10.0 MHz
Mixer:	39.56 MHz
Sampling Rate:	40.00 MHz
Burst Decimation:	2
Analog Threshold:	100.00 mV
Burst Detector Start Min:	2
Burst Detector Start Max:	14
Burst Detector End Min:	4
Burst Detector End Max:	8
AB Phase Cal.:	-3.57 °
AC Phase Cal.:	-7.52 °
BC Phase Cal.:	-3.95 °
Auto-Setup Enabled:	No
Enabled:	Yes

**Misc.**

Start Date: 01/30/2013 at 02:25:54 ms

Stop Date: 01/30/2013 at 02:26:33 ms

Data Library

Device Controls

Results

Export

Message sent: Command: subscr

Figure 9.8: ASA Processor settings.

Figure 9.8 shows the screen that provides a summary of the ASA signal processor settings for this measurement point. This information is saved with the data file and allows the user to recover the settings for that data and if desired, repeat the measurements with those settings.

### LDV/PDI Optics

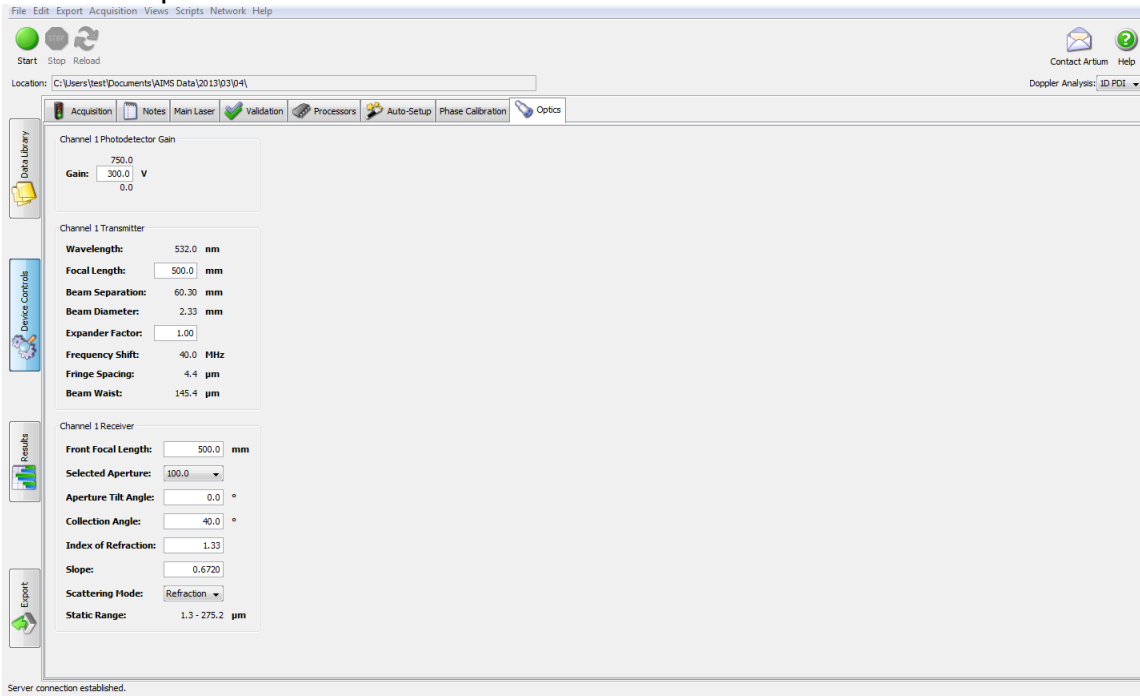


Figure 9.9: LDV/PDI Optics Settings.

## Optics Cleaning

Cleaning optics should only be done when necessary. It is not necessary to clean the lens if it just has a few visible specks of dust. Overly frequent or aggressive cleaning can actually damage and prematurely age the special coatings on mirrors and lenses—permanently degrading their performance.

When optics are truly dusty or dirty, that's when they need to be cleaned. The best philosophy is progressive: clean only as much as you need to clean, starting with the gentlest cleaning and then progress to more thorough cleaning using more force. Clean outside optical surfaces first before even considering disassembly and cleaning inner surfaces.

Note: These techniques are for normally dusty optics or those with minor fingerprint or smudges. Optics with films, fungus, oil or grease need special techniques for cleaning.

For basic cleaning:

1. Use clean, dry compressed gas or compressed air to blow off loose dust and large particles. This greatly reduces your chances of scratching the lens or mirror in successive steps and may be all that's needed. Canned gases like Dust-Off contain bitterants and other compounds that can plate out or leave deposits unless proper precautions are taken. Never shake a can of compressed gas before using it and always first vent a jet of gas away from any optics. Use the can in an upright position and move it slowly or move the optics instead. Compressed air should be filtered and also first be jetted away from any optics to blow out any dust in the line.

2. Use a cleaning solution to gently lift off any remaining dirt or smudges. The recommended solvent is alcohol (isopropyl or methanol). You can make a mix from pure alcohol and distilled water or buy off-the-shelf dilutions from your local drugstore. Dilutions of 50 to 70 percent alcohol work best. Higher percentages evaporate too fast and have a greater chance of dissolving optical cements, non-metallic parts and lacquers on mechanical parts if the solution accidentally gets into the wrong parts of the optics. Lower percentage dilutions won't evaporate readily but may still cause problems if the solution accidentally gets into the wrong parts of the optics. The alcohol can be used straight or you can add one or two drops of clear liquid dish-type soap (non-waxy) per quart to help lift off dirt and finger oils. (Adding too much soap will leave visible residues on your optics.)

3. Use the solution to wet soft, plain tissue or cotton balls for larger optical surfaces or cotton swabs for small parts. Also available from camera stores and optics suppliers are optical

cleaning tissues that are soft and lint-free. Don't use too much solution, as you don't want excess fluid to run off the surface you're cleaning.

For the primary lens or mirror, use a wet cotton ball or tissue and gently drag it across the surface in straight strokes. Simply dragging it is the lowest force possible and the least chance of scratching from any remaining dust. Repeat with new balls/tissues. If you must use force (on a localized deposit), use as little as you can, just enough to remove the deposit, no more, without damaging the optical surface.

4. If a film is forming on the outside of the lens, it is recommended, if possible, that the user should unscrew and remove the lens cell from the optics package (Transmitter, Receiver, Transceiver), then remove the glass lens from the cell. This requires a tool called a spanner wrench (see picture) that allows the retainer ring to be removed. With the lens removed, it is much easier to apply the solvent and clean the lens to the edges. This is not hard to do, but care must be taken in the handling of the lens so it is not dropped and no fingerprints are added. Wear latex gloves and/or handle the lens only by the edges. Also, the lens is asymmetric - it must go back into the cell exactly the way it was removed. The system performance will degrade if the lens is put in backwards.



Spanner Wrench to remove lens retainer rings

## Appendix I

### *PDI Calculations*

This chapter describes the methods by which the software interprets the raw information received from the instrument and computes information to obtain droplet velocity and size. The software resolves the stored raw data into the velocity and size measurements for each particle and then computes the remaining statistical parameters. This section describes the calculations completed by the computer. The nomenclature for this chapter is as follows:

$\Delta$	Spatial Wavelength
$\delta$	Fringed Spacing
$\phi_{12}, \phi_{13}, \phi_{23}$	Phase shift in degrees between detectors 1 and 2, 1 and 3, and 2 and 3 (also called A, B, and C)
$\theta$	Receiver Collection Angle
$\gamma$	Laser Beam Intersection Angle
$\alpha, \alpha_r$	Aperture width, resultant aperture width
$D_{max}$	Diameter of the largest particle size
$D_{10}, D_{20}, D_{30}, D_{32}$	Mean particle diameters: Arithmetic, Area, Volume, Sauter
$d$	Diameter of spherical particle
$f, f_D, f_m, f_r, f_s, f_t$	Frequency: Doppler, mixer, raw, shift, transformed
$I, I_i, I_o, I_s$	Light Intensity: incident, maximum at $r = 0$ , scattered
$i$	Histogram Bin Number
$j$ or $n$	Number of samples in histogram bin
$K$	Optical constant
$ND$	Number Density
$n, n_c$	Number of samples in each bin: corrected size count
$PA$	Probe Area
$PV$	Probe volume That
$PVC$	Probe Volume Correction
$PVO$	Probe volume cut off
$RL_1, RL_2$	Receiver Lenses: Collimating, Focusing focal lengths
$r_w$ or $w$	Laser beam radius measured from the centerline of the beam: $I = I_o/e^2$
$S, S_{12}, S_{13}$	Effect of detector separations: between detectors 1 and 2, and 1 and 3
$\Sigma$	Sizing Slope Factor



$\tau$	Particle or droplet transit time through the probe volume
$t, t_{tot}$	Time: total run time
$v$	Velocity
<b>VF or F</b>	Volume Flux

## Velocity Measurement

The particle velocity is measured by the method typically used for laser Doppler velocimetry. That is, as a particle crosses the interference fringes created by the two intersecting coherent laser beams, Figure A1.1, it refracts or reflects the local light intensity onto the receiver. The light intensity pattern projected onto the receiver and directed to the photomultiplier tubes produces a typical Doppler burst signal, Figure A1.2. The signal consists of a high frequency Doppler component superimposed upon the low-frequency Gaussian pedestal component. The frequency of the signal is directly related to the velocity of the particle through the relationship

$$v = f_d \delta$$

The fringe spacing of the interference pattern is determined by the wavelength of the laser beam and the beam intersection angle and is given by the following expression

$$\delta = \frac{\lambda}{2 \sin(\gamma / 2)}$$

The raw signal produced by the photodetectors and received by the signal processor is a combination of the Doppler frequency and the shift frequency produced by the presence of a Bragg cell. The signal frequency is given as

$$f_r = f_D + f_s$$

The raw signal is passed through a high pass filter set at 10 MHz (or 20 MHz) to remove the pedestal component of the Doppler burst signal and any low-frequency noise. The signal is then combined with the mixer frequency and sent through a low pass filter to eliminate the high frequency components including the sum frequency from the mixer and any high-frequency noise. The remaining frequency is given as

$$f_t = f_r - f_m$$

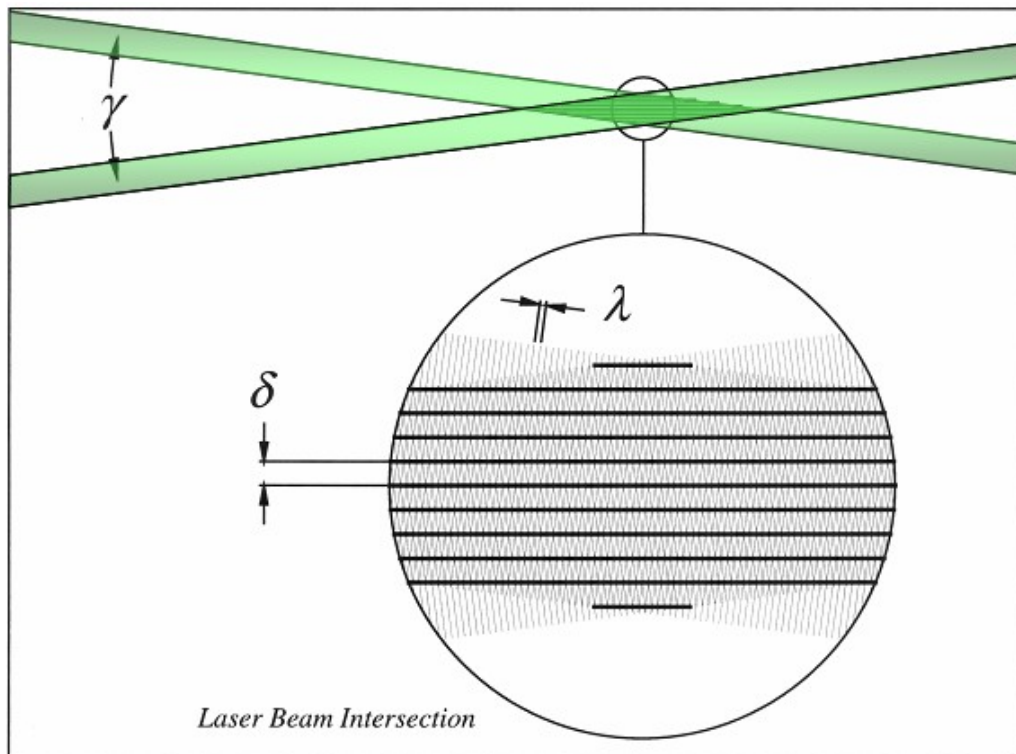


Figure A1.1: Schematic showing the laser beam intersection and the formation of interference fringes in the probe volume.

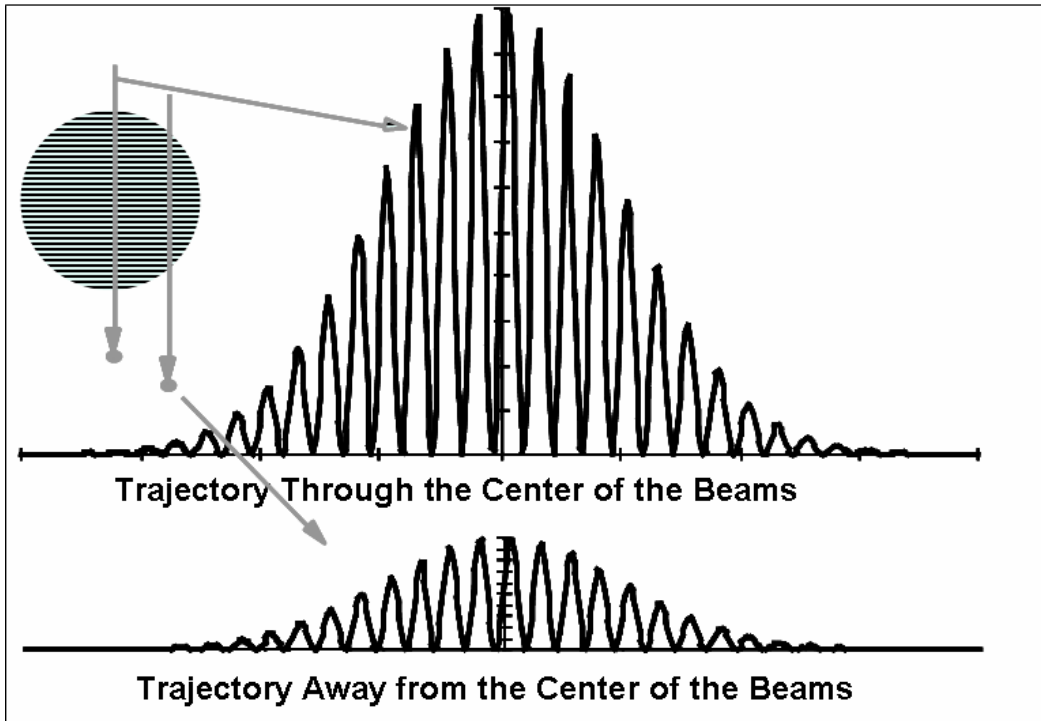


Figure A1.2: Simulated Doppler signals.

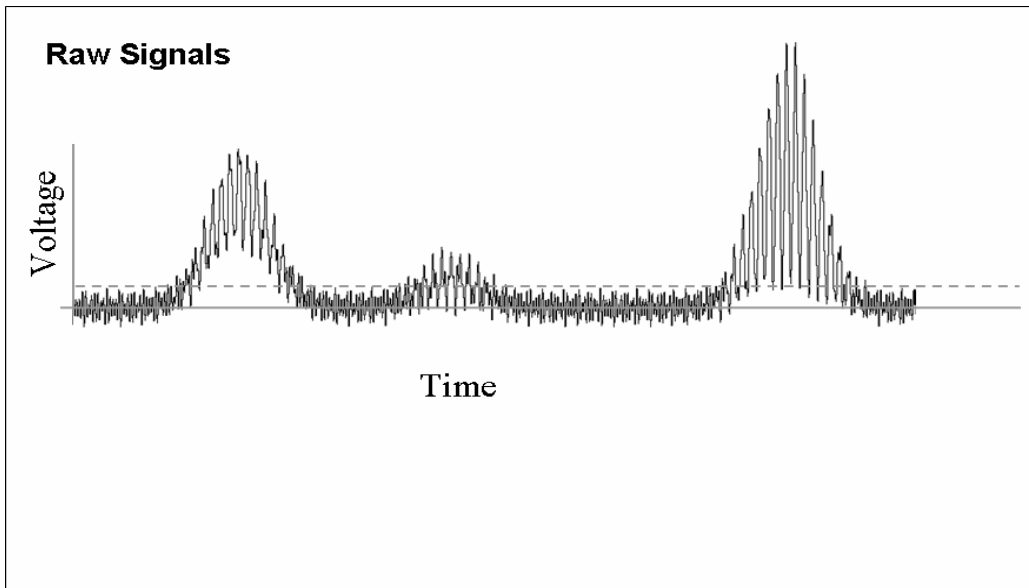


Figure A1.3: Typical Doppler burst signals for different trajectories through the probe volume.

This frequency is processed using the FFT programmed in the system computer. The Doppler frequency is then obtained from the known mixer and shift frequencies and measured raw frequency using following expression

$$f_D = f_t + f_m - f_s$$

## Size Measurement

This section describes how the diameter of the particles is determined using the phase Doppler interferometer method. The particle magnifies the interference fringe pattern onto the receiver to different degrees relative to a particle size. The degree of magnification is measured by comparing the spacing of these fringes on the receiver detectors (spatial wavelength  $\Delta$ ) and the fringe spacing. The diameters of the particles are determined using this relationship along with the receiver focal length and the sizing slope factor given as

$$d = \frac{F\delta_r}{s\Delta}$$

A spatial wavelength,  $\Delta$  is determined by using the phase shift of the signal between the detectors in the time domain along with the calibrated spacing of the detectors. The spatial wavelength,  $\Delta$  is obtained from the weighted average of

$$\bar{\Delta} = 360 \left[ \frac{k_{12}S_{12}}{\phi_{12}} + \frac{k_{13}S_{13}}{\phi_{13}} + \frac{k_{23}S_{23}}{\phi_{23}} \right] / [k_{12} + k_{13} + k_{23}]$$

Artium Technologies, Inc. uses several proprietary methods for resolving the sizing slope factor for all possible transmitters/receiver configurations. The slope is calculated assuming spherical particles and therefore, the particles to be sized should be spherical or near spherical if accurate results are to be obtained.

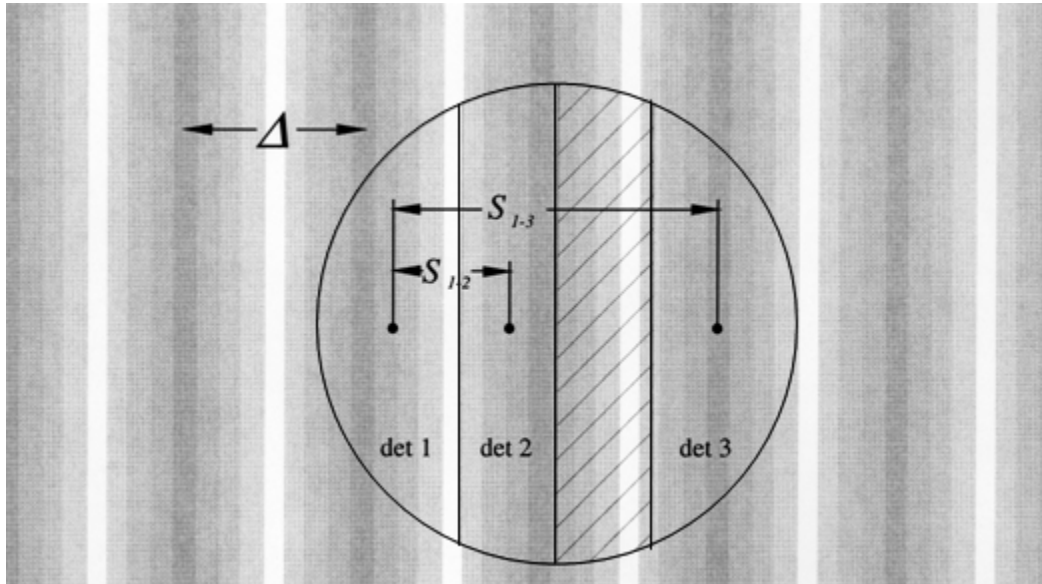
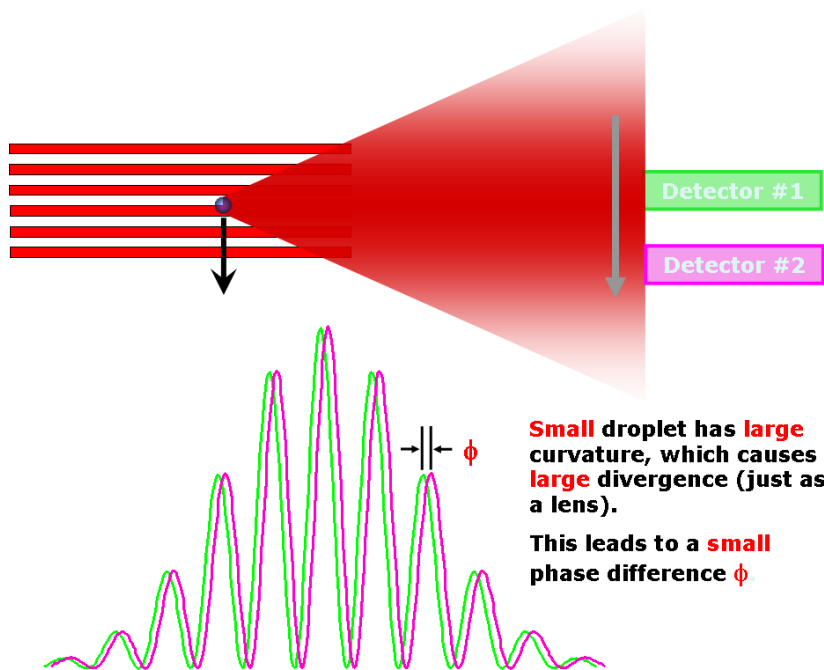


Figure A1.4: Schematic showing the interference fringes produced by the scattered light and projected onto the receiver lens.



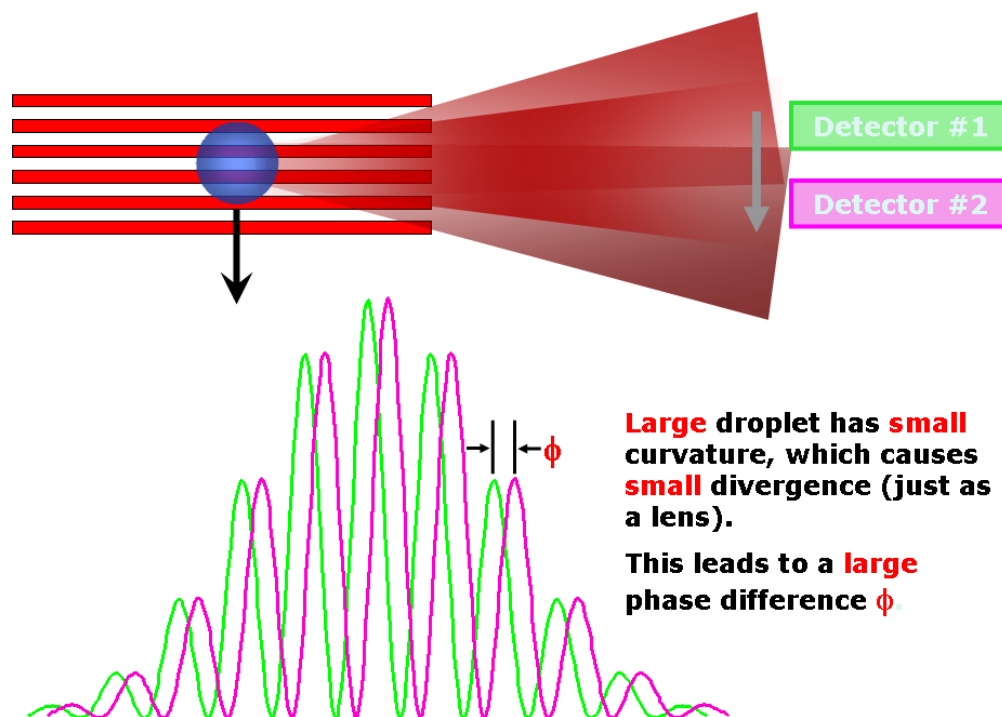


Figure A1.5: Schematic showing the interference fringes formed by the scattered light and the pattern overlaid on the receiver lens and a description of how the droplets produce different phase shifts at the pairs of detectors.

### Probe Volume, Probe Area, and Probe Volume Correction

The probe volume is a volume through which particles must pass to be measured by the PDI systems. Probe volume is defined by the focused laser beam diameter and the slit aperture width in the receiver. The shape of the probe volume can be estimated as a slice of a cylinder with oblique ends. The width and angle of the slice are determined by the slit aperture width in the receiver, optics, and the angle of the receiver relative to the transmitted beams. The intersecting beams are at a small enough angle such that they can be assumed as cylindrical in shape within the region seen by the receiver.

The cylindrical diameter of the probe volume increases in diameter for increasing size classes of particles. This is due to the relation between the amount of incident light scattered by particle (proportional to the diameter of the particle squared) and particle size in conjunction with a Gaussian nature of the laser beam intensity profile illuminating the particles. The amount of light incident on the particle is determined by the distance the particle passes from the center of the laser beams and its location along the trajectory through the beams. For two intersecting laser beams the incident light is

$$I_i(r) = I_o e^{\frac{-2r^2}{r_w^2}}$$

The intensity of the light scattered by particle is proportional to the particle surface area. Combining the size relation with the above Gaussian equation results in the expression

$$I_s(r, d) = KI_i(r)d^2 \approx KI_o e^{\frac{-2r^2}{r_w^2}} d^2$$

which is equal to the amount of light incident on the receiver optics relative to a particle size and position.

A minimum amount of light incident on the receiver is needed in order for the instrument to detect a particle. This intensity cut off determines the maximum radius  $r$  at which each particle size can be detected yielding a cylindrical diameter  $D$  as a function of the ratio of the probe volume diameters to particle diameter is

$$D^2(d) = D_{\max}^2 - 4r_w^2 \ln\left(\frac{d_{\max}}{d}\right)$$

which is used when calculating the probe volume correction, PVC.

The maximum probe diameter is either assumed to be equal to a nominal value by using an analytical method for probe volume correction or is determined in situ by the transit time method. The transit time is the time a particle spends in the probe volume which depends on its speed and the diameter of the probe volume. The measured transit time multiplied by the particle velocity yields the particle path length within the probe volume. Artium Technologies Inc. uses a proprietary method of combining the transit time of all particles passing through the probe volume to determine the maximum probe diameter.

The probe area is determined from the maximum probe diameter of the maximum size bin and is given as

$$PA = \frac{D_{\max} a_r}{\sin \varphi}$$

The resultant aperture size at the laser beam intersection is related to the aperture size within the receiver and the focal lengths of the receiver lenses. The resultant aperture size is given as

$$a_r = a \left[ \frac{RL_1}{RL_2} \right]$$

The number of particles in each size class of the distribution is multiplied by the probe volume correction factor to reflect the change in sampling volume with particle size and is given as

$$n_c(d) = n(d)PVC(d)$$

The probe volume correction factor is simply the ratio of the probe area for the maximum particle size bin ratio to the probe area of each individual size bin  $d$ . Since the aperture and the angle of light scatter detection,  $\Theta$ , remain constant, the ratio is determined only by the maximum probe diameter of each particle size class.

$$PVC(d) = \frac{D_{\max}}{D(d)}$$

The in situ probe volume measurement and correction is dependent on certain factors in order to perform properly. First, the laser beams must have a nearly Gaussian intensity distribution at the beam intersection. The trajectory of the particles should be predominantly normal to the direction of the beams for a two component system (two orthogonal velocity components measured). For a one component system, the predominant trajectory of the particles should be in the direction of measurement of the velocity. If these conditions are not met the analytical method to define the probe volume correction may be more accurate.

### Mean and Median Calculations

In this section, the various mean diameters used in the presentation of data are presented. These mean values are commonly used in spray analysis.



Arithmetic or Linear Mean Diameter (D10)	$D_{10} = \frac{\sum_i n_{c(i)} d_i}{\sum_i n_{c(i)}}$
Area Mean Diameter (D20)	$D_{20} = \sqrt{\frac{\sum_i n_{c(i)} d_i^2}{\sum_i n_{c(i)}}$
Volume Mean Diameter (D30)	$D_{30} = \sqrt[3]{\frac{\sum_i n_{c(i)} d_i^3}{\sum_i n_{c(i)}}$
Sauter Mean Diameter (D32)	$D_{32} = \frac{\sum_i n_{c(i)} d_i^3}{\sum_i n_{c(i)} d_i^2}$
Total Number	$tN = \sum_i n_{c(i)}$
Number Fraction	$fN = \frac{\sum_i n_{c(i)}}{tN}$
Total Length	$tL = \sum_i n_{c(i)} d_i$
Length Fraction	$fL = \frac{\sum_i n_{c(i)} d_i}{tL}$
Total Surface	$tS = \pi \sum_i n_{c(i)} d_i^2$
Surface Fraction	$fS = \frac{\pi \sum_i n_{c(i)} d_i^2}{tS}$
Total Volume	$tV = \frac{\pi}{6} \sum_i n_{c(i)} d_i^3$
Volume Fraction	$fV = \frac{\frac{\pi}{6} \sum_i n_{c(i)} d_i^3}{tV}$

### Number Density and Volume Flux Measurements

Number Density is a measurement of the number of particles per unit volume present in the measurement space. There are two methods used to calculate number density and they are referred to as the swept volume method and the transit time method. The total corrected count (corrected for probe volume) is divided by this volume to calculate the number density and is given as

$$ND = \frac{1}{(PA)(t_{Tot})} \sum_i \frac{n_{c(i)}}{|v_i|}$$

A separate average absolute velocity is calculated for each size bin to eliminate the velocity biasing on the sampling statistics and is given as

$$|v_i| = \frac{\sum_j |v_{i,j}|}{n}$$

With the transit time method which is favored, the number density is determined using the transit times for the particles as they pass the sample volume. The transit time is the measure time that the particle spends within the probe volume. This method uses the computed ratio of time duration when there is a particle in the probe volume to the total sample time for the measured distribution at that point. Transit time ratio divided by the probe volume yields the number density given as

$$ND = \frac{1}{t_{Tot}} \sum_i \frac{\sum_j Tt_{i,j}}{PV_i}$$

This method is applied for each size class to accommodate the size biasing of the probe volume as a function of drop size.

Both methods rely on an accurate probe area calculation. The transit time method will work best as long as the beams are partially Gaussian at the intersection. The swept volume method works well if the trajectories of the particles are normal to the direction of the beams in a two component system or if the trajectories of the particles are in the direction of the velocity component measured for a one component system.

Volume flux is calculated using the following expression

$$VF = \frac{tV}{t_{Tot}PA} = \frac{\pi tND_{30}^3}{6 t_{Tot}PA}$$

Mass flux can be calculated by multiplying the volume flux by the density of the spray drops or particles being measured.

## Liquid Water Content (LWC)

The liquid water content is the volume of liquid water in a given volume of space. Liquid Water Content in  $\text{gm/m}^3$  is given as

$$LWC = \frac{\pi}{6} \rho D_{30}^3 ND$$

where  $\rho$  is the density of the liquid.

## Appendix II

### *Phase Doppler Interferometry Theory of Operation*

Bachalo (1980) theoretically described the light scattering from spherical particles and showed that the phase shift of the light scattered from two intersecting beams could be used to accurately and reliably measure the diameter of spherical particles. With the use of pairs of detectors to enable the measurement of the interference fringe pattern formed by the far field interference of the scattered light, a method for reliably and accurately measuring spray drop size even in difficult measurement environments was realized, Bachalo and Houser (1984). Following the initial development of the phase Doppler interferometry method, significant research and development has been devoted to the improvement of this important instrument and numerous publications have been written on the subject [Bachalo et al. (1993); Dodge (1987)]; Sankar et al. (1991); Sankar and Bachalo ((1995); Bachalo and Sankar (1988); Bachalo and Houser (1985); Bachalo et al. (1988); Ibrahim et al. (1990); Ibrahim et al. (1991); Ibrahim and Bachalo (1992); Ibrahim and Bachalo (1994);].

The Phase Doppler Interferometer (PDI) instrument, formerly known as the Phase Doppler Particle Analyzer (PDPA), has advanced as the standard laser-based diagnostic instrument for simultaneously measuring the size and velocity of individual spherical particles in poly-disperse flow environments.

The success of the method may be attributed to the measurement principles upon which it is based, namely, light scattering interferometry. Light scattering interferometry utilizes the wavelength of light as the measurement scale and, as such, the performance is not as easily degraded as it is for systems using light scattering intensity information for the estimation of the particle size. In addition, the method does not require frequent calibration. Over the decades, the instrument has proven to need only an initial factory calibration. The parameters affecting the measurement which include the laser wavelength, beam intersection angle, transmitter and receiver focal lengths, and the detector separation do not change with age and require deliberate intervention by the user or serious mistreatment of the instrument before they lose adjustment. Another important characteristic of the method that is often missed is related to the signals generated by the device. Unique sinusoidal signals are produced which can be easily detected even in the presence of noise using the Fourier analysis.

As an aid to understanding the measurement method, it will be useful to consider the simplest form of light scattering by a sphere. A geometrical optics description of the light scattering phenomena is illustrated in Figure A2.1. At the first interface, part of the incident

light is reflected from the surface of the sphere and these rays are referred to as  $p = 0$  following the convention of van de Hulst (1957). The light transmitted and refracted by the sphere is referred to as  $p = 1$  rays and rays reflected from the interior surface and refracted in the backward direction are  $p = 2$  rays. The relative light energy reflected from and transmitted through the sphere may be calculated using the Fresnel reflection coefficients.

A schematic of the optical and electronics components for a basic PDI system is presented in Figure A2.2. The optical requirements are identical to that of a one-component laser Doppler velocimeter (LDV), except that three detectors are used in the receiver, and the receiver must be located at a known off-axis angle to the transmitted beams. The preferred light collection position for the receiver is at an off-axis angle of from 25 to 45 degrees to the transmitted beam direction measured from a plane passing through the two intersecting beams. The optical axis of the receiver should be in a plane that passes through the intersection of the beams, and is orthogonal to the plane formed by the two intersecting beams. Other receiver angles and configurations have been suggested but we do not recommend that they be used unless no alternative exists due to some other constraints of the experiment.

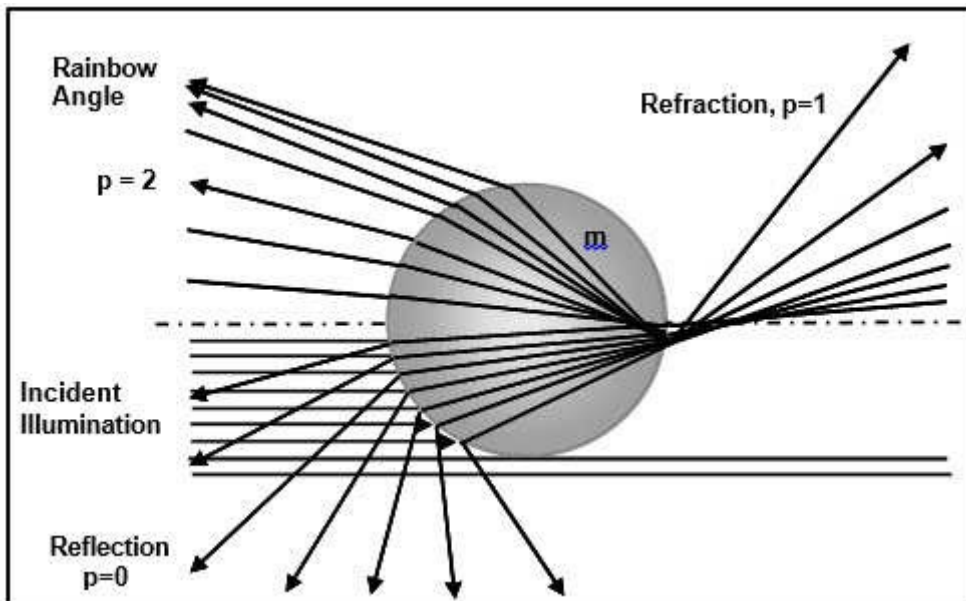


Figure A2.1. Simple ray diagram showing the deflection of the light rays incident on a spherical particle illustrating the  $p = 0, 1, 2,$  and  $3$  rays.

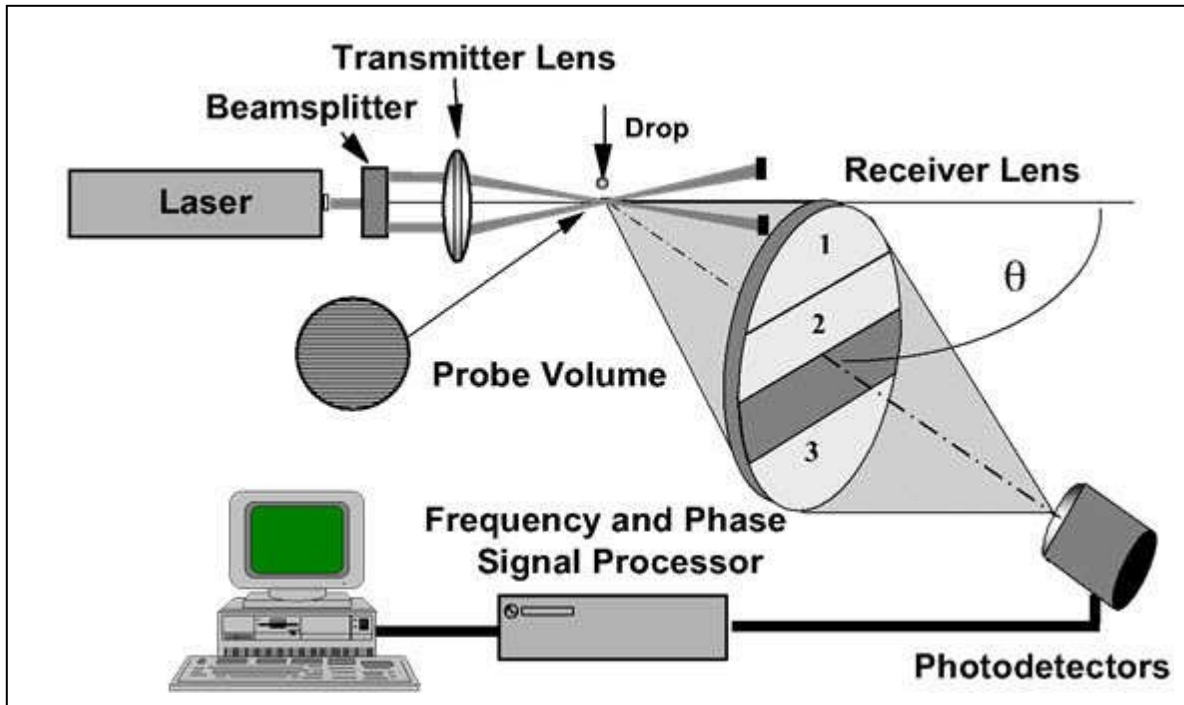


Figure A2.2. Schematic of the basic Phase Doppler Interferometer (PDI) system.

In the basic PDI optical system, the laser beam is split into two beams of equal intensity. The beams are then focused and made to intersect using a transmitter lens. Frequency shifting is used to compress the frequency dynamic range and resolve the direction ambiguity that would occur for drops passing in a reverse direction. Particles passing through the beam intersection will scatter light that is collected by the receiver lens. A single aperture is used in the receiver to allow only light scattered by particles crossing a small region of the beam intersection to reach the photodetectors. Shown in Figure A2.3 is a schematic depicting a spherical particle located at the intersection of the two laser beams. An enlarged view of the sphere with a light ray from each beam incident upon it is also shown. Since the rays from each beam enter at different angles, they must pass on different paths to reach a common point P. The sphere has an index of refraction,  $m$ , that is different than the surroundings. Thus, the difference in the optical path length of ray 1 from beam 1 relative to ray 2 from beam 2 will produce a phase shift between light waves traveling in the directions shown by ray 1 and ray 2 to the point P. An interference fringe pattern will form in the distant space surrounding the drop. Under ideal conditions, the interference fringe pattern will have a sinusoidal intensity distribution and will form a hyperbolic set of curves when projected onto a plane. The wavelength of the pattern at a given location will be inversely proportional to the drop diameter. This phase shift can be calculated easily and exactly using the geometrical optics theory. Given a specific location

in space (points on the receiver lens aperture) the phase shift between the light scattered from each beam will vary in proportion to the drop diameter.

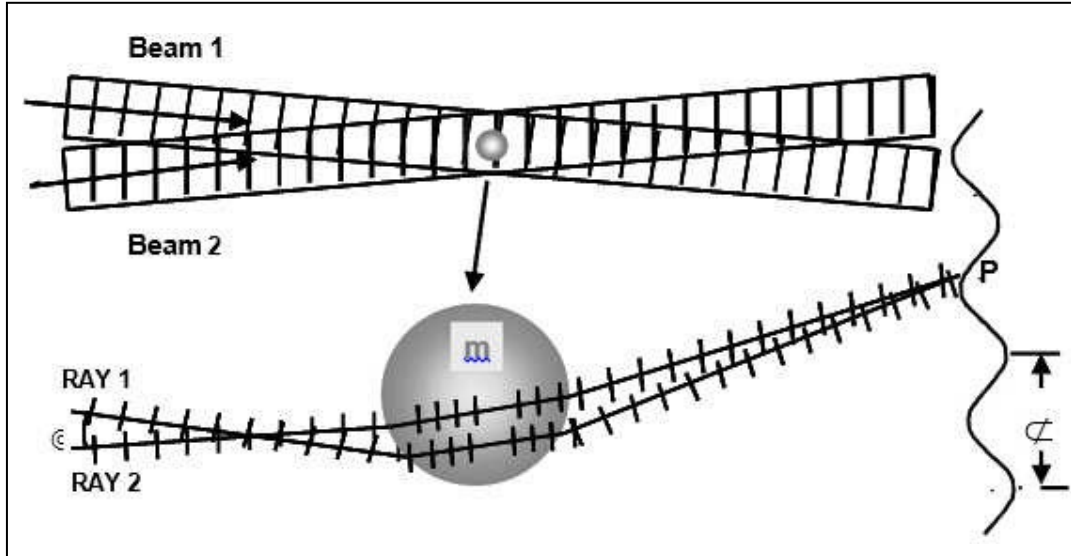


Figure A2.3. Simple diagram showing the light rays and waves incident on a spherical particle and the phase shift resulting from the passage of the light through the drop on different optical paths.

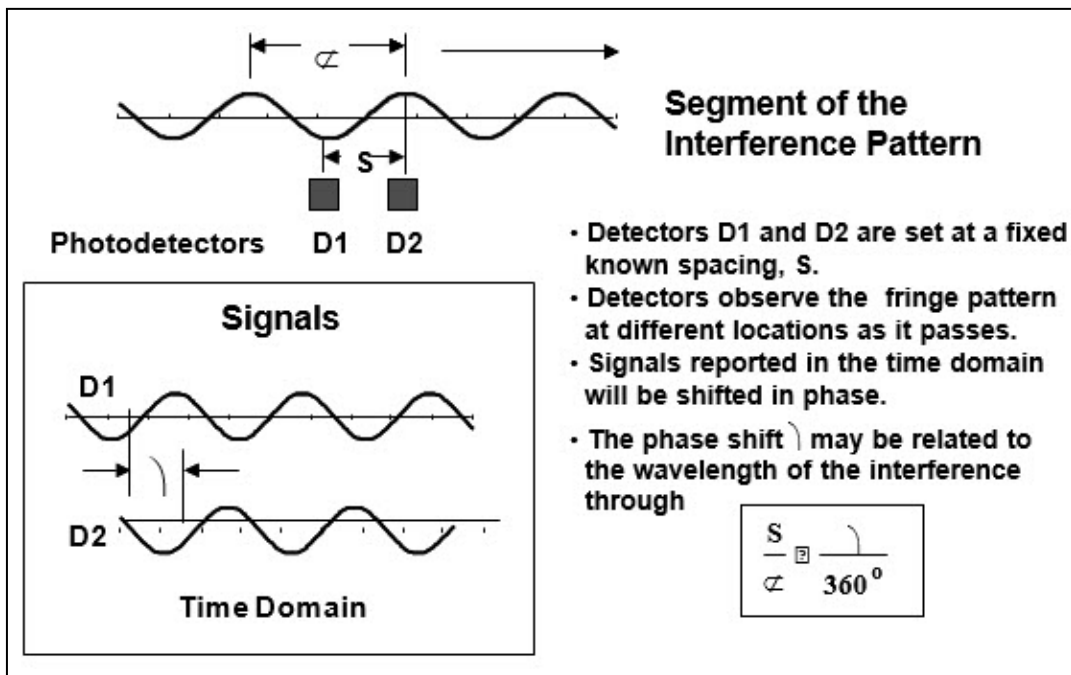


Figure A2.4. Scheme used for rapidly measuring the spacing, L of the interference fringes produced by the scattered light.

Measurement of the spacing of the interference fringes produced by the scattered light is accomplished in a straightforward manner using pairs of detectors, Figure A2.4. For this approach, pairs of detectors are located in the fringe pattern, or an image of it, and the separation  $S$  between the detectors is known. When the particle or drop is moving, the usual Doppler shift in the frequency of the scattered light occurs. The difference in the Doppler frequency shift between the light scattered from beam 1 and beam 2 causes the fringe pattern to appear to move.

As the pattern sweeps past the detectors at the Doppler difference frequency, each detector produces a signal that is similar in frequency but shifted in phase. The phase shift is related to the spacing of the scattered fringe pattern through the following relationship:

$$\frac{s}{\Lambda} = \frac{\phi}{360^\circ}$$

where  $s$  is the detector spacing and  $\phi$  is the phase shift between the signals. The wavelength  $\Lambda$  is the spacing of the interference fringes formed by the scattered light and is inversely proportional to the drop diameter. Three detectors are used to avoid ambiguity in the measurements, to provide redundant measurements of the pattern, and to improve the resolution for the small particles. The ambiguity could occur when the fringe spacing, is less than the detector separation. In this case, the phase shift would be greater than 360 degrees but is reported as  $\phi - 360$ .

A unique three-detector separation arrangement originally invented by Bachalo (US Patent 4,540,283) and first reported in 1982 (NASA Technical Report) is shown in Figure A2.5. The phase versus diameter curves that correspond to these detector separations are also shown. With this configuration, the phase shift between the signals from the closely spaced detectors, D1 and D2 follow the smaller slope on the phase-diameter plot indicated by the dotted lines. The phase between the signals for the detectors with the larger spacing, D1 and D3, follow the curves with the greater slope. With this arrangement, the phase may be measured for detector separations that extend over several fringes (1 fringe corresponds to a measured phase shift of  $360^\circ$ ) when placed in the field of the scattered light. More recently (patent pending), Bachalo has reported the use of three pairs of detectors (12, 13, and 23) to be used in the measurement as shown in the updated diagram of phase versus diameter.



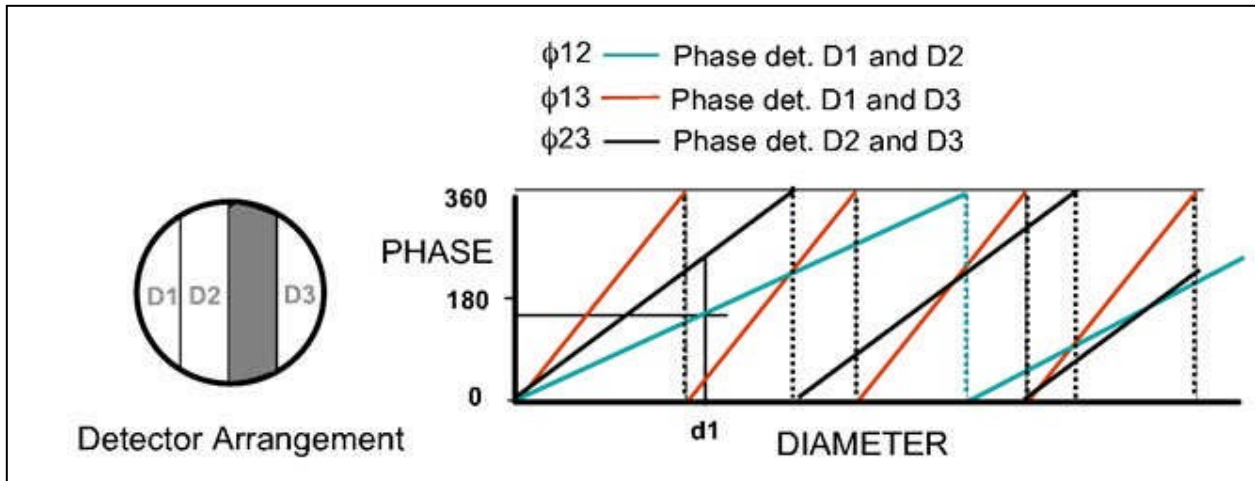


Figure A2.5. Three-detector configuration and the resulting phase diagram used to avoid ambiguity and extend the measurement range with high resolution (Patent Pending).

It is relatively easy to see that the interference fringe pattern produced by reflection will appear to move in the opposite direction to that produced by refraction. With the three detectors set to detect the phase shift for refraction, as shown in Figure A2.6, the correct phase shifts for 12, 13 and 23 will be detected. However, when the dominant light scatter is by reflection, the wave will travel in the opposite direction. For this case, the relationship between 12, 13, and 23 will no longer pass the phase comparison criteria so these samples will be rejected.

Unfortunately, spray droplets will also pass on trajectories through the Gaussian beam, which will result in a significant superposition of scattered light intensity by reflection and refraction. In this case, the resultant interference fringe pattern is no longer a pure sinusoidal wave but a superposition of several interference patterns. Additional means are required to reject particles passing on these trajectories to avoid or minimize measurement errors. Bachalo (1980) recognized this problem, and it was the primary reason for selecting the 30° light scatter detection angle wherein refraction is approximately 80 times the reflection (assuming a uniformly illuminated sphere). Bachalo and Houser (1984) addressed this problem experimentally by traversing monodisperse drops along controlled trajectories within the measurement probe volume for a range of drop-size-to-beam-diameter ratios. Fortunately, the redundant phase information coupled with other information has been proven successful in mitigating or eliminating this source of measurement error.

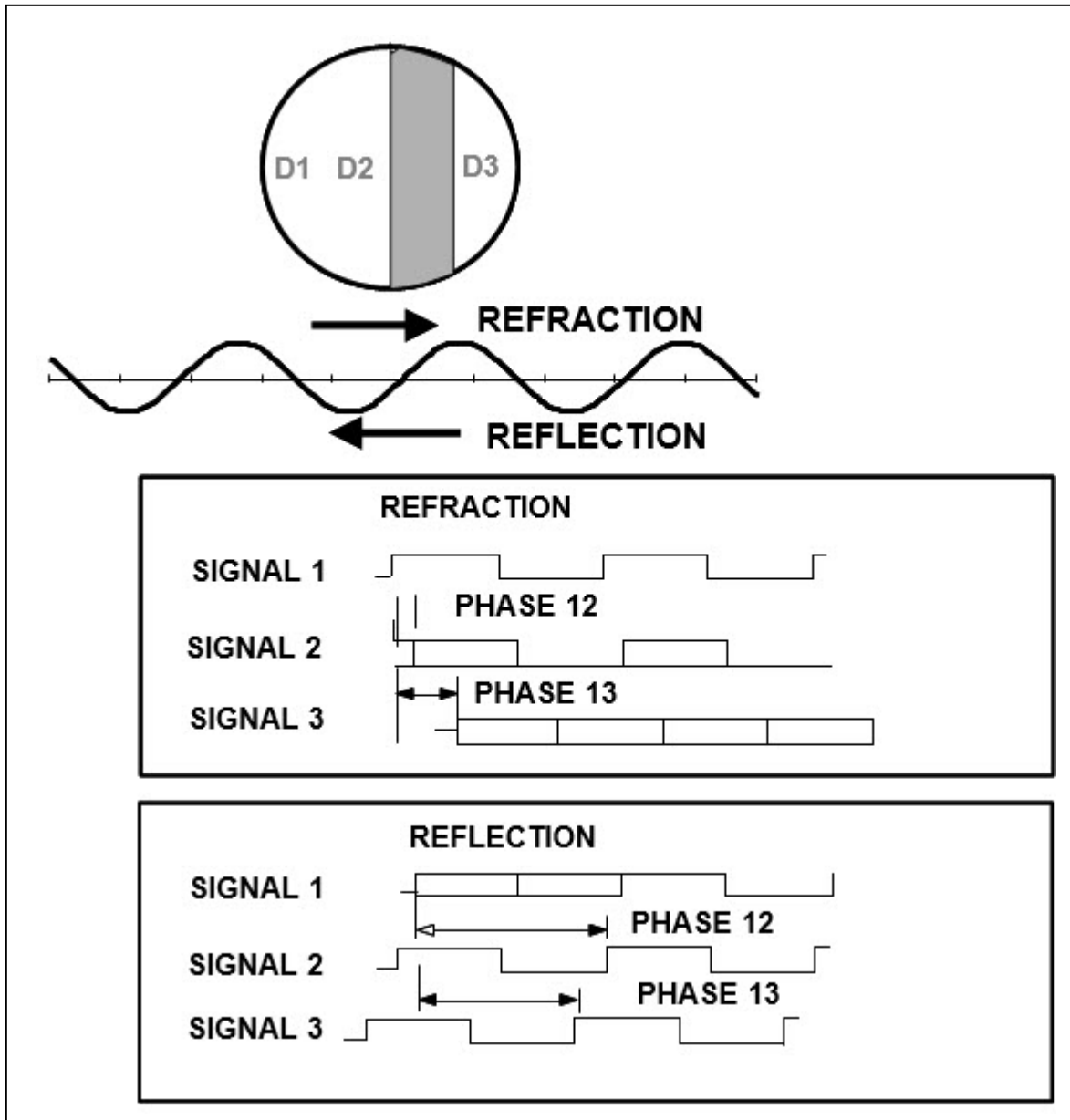


Figure A2.6. Three-detector configuration used by Bachalo, 1982 to resolve the phase ambiguity and to extend the measurement range and resolution.

The key parameter in the analysis of this problem is the drop diameter-to-beam diameter ratio,  $r = d/D_0$  where  $d$  is the drop diameter and  $D_0$  is the diameter of the focused beams at the sample volume, Figure A2.7. At this point, it is useful to consider the problem in three regimes: particles smaller than the focused beam diameter, ( $r \ll 1$ ) particles similar in size ( $r \sim 1$ ), and particles larger than the beam diameter ( $r \gg 1$ ). In the first case, the particles can be assumed to be approximately uniformly illuminated so the trajectory error is not a problem. In the case of the particles being of similar diameter to the focused beam diameter, the trajectory problem is most difficult since the scattering intensities from

reflection and refraction can be of similar order producing a complex interference fringe pattern with a progressively increasing magnitude of error. If the particles are larger than the focused beam diameter, then either reflection or refraction will dominate the scattering. For this case, the phase ratio will be effective in rejecting signals produced by the wrong scattering component.

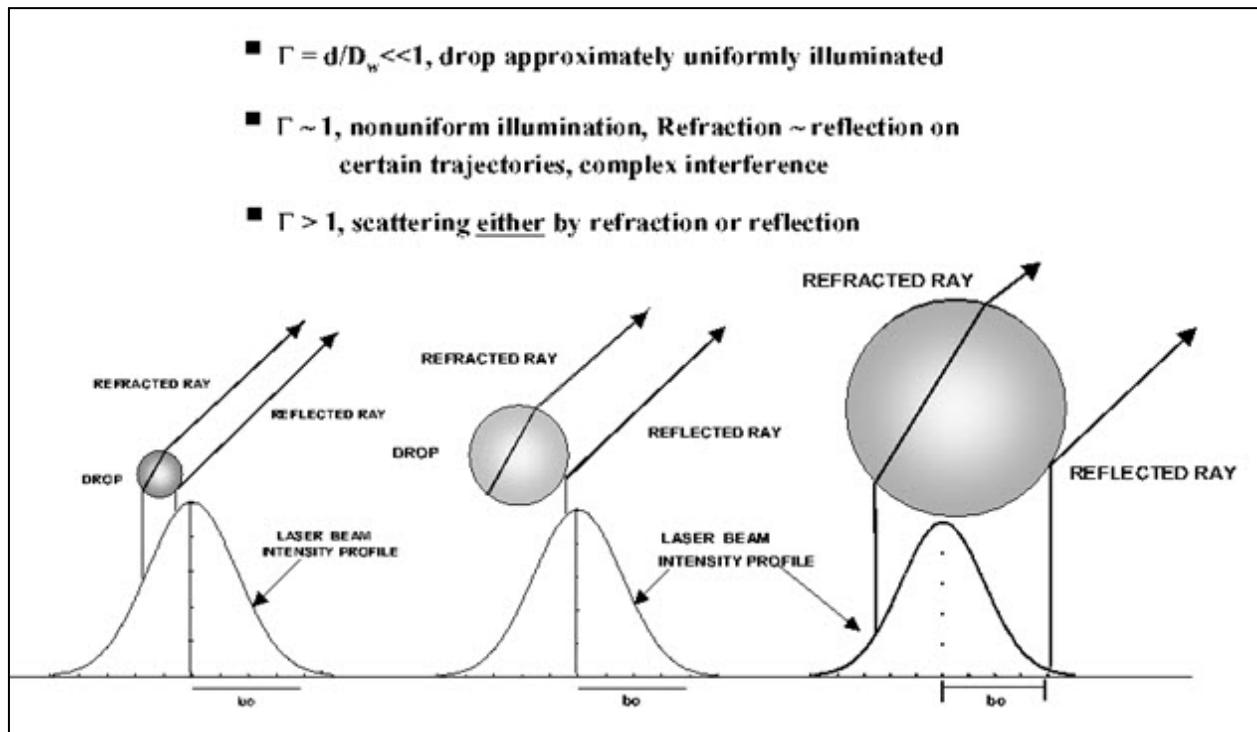


Figure A2.7. Schematic illustrating the three drop size cases passing a Gaussian beam;  $r \ll 1$ ,  $r \sim 1$ , and  $r > 1$ .

Sankar et al. (1992) have shown that the trajectory-dependent sizing errors can be minimized by the proper selection of the optical parameters, namely, the beam intersection angle and using the two-detector-pair arrangement of the PDI. This work represented the first recognition of the importance of the relative phase difference between the reflected and the refracted light in resolving the trajectory-dependent error problem. Increasing the beam intersection angle serves to increase the difference between the phase of light scattered by refraction and reflection, allowing a more effective discrimination using the phase ratio from the two pairs of detectors. In a later paper by Sankar et al. (1995), it was shown that with the proper selection of the optical parameters, the phase Doppler response for particles passing along the error-prone trajectories could be forced to always result in a size over-prediction, if at all, and never an under prediction.

This information can then be used in conjunction with the scattered light intensity level for each particle to eliminate the erroneous measurements (Bachalo, US Patent 4,986,659).

The intensity validation method is based on the observation that when particles pass on the “bad” trajectories near the edge of the beam, the incident intensity and hence, the scattered light is at least an order of magnitude lower than for particles passing on a trajectory through the center of the beam. In addition, if the light scattering by reflection is detected, the signal will be approximately two orders of magnitude lower than for the light scattered by refraction because of the lower light scattering efficiency. Thus, calculating a minimum acceptable light intensity level for each size class and measuring the signal amplitudes along with the drop size can provide information for eliminating the particles passing on the trajectories susceptible to errors from consideration. Using this approach, the definition of the edges of the sample volume are better defined at higher levels than is possible on the wings of the Gaussian wherein a small uncertainty in amplitude corresponds to a large change in the size of the sample volume. Detailed experimental studies and theoretical simulations have been conducted to evaluate the reliability of the intensity validation method. Sankar et al. (1995) and Strakey et al. (2000) have shown that the method is effective in controlling trajectory errors.

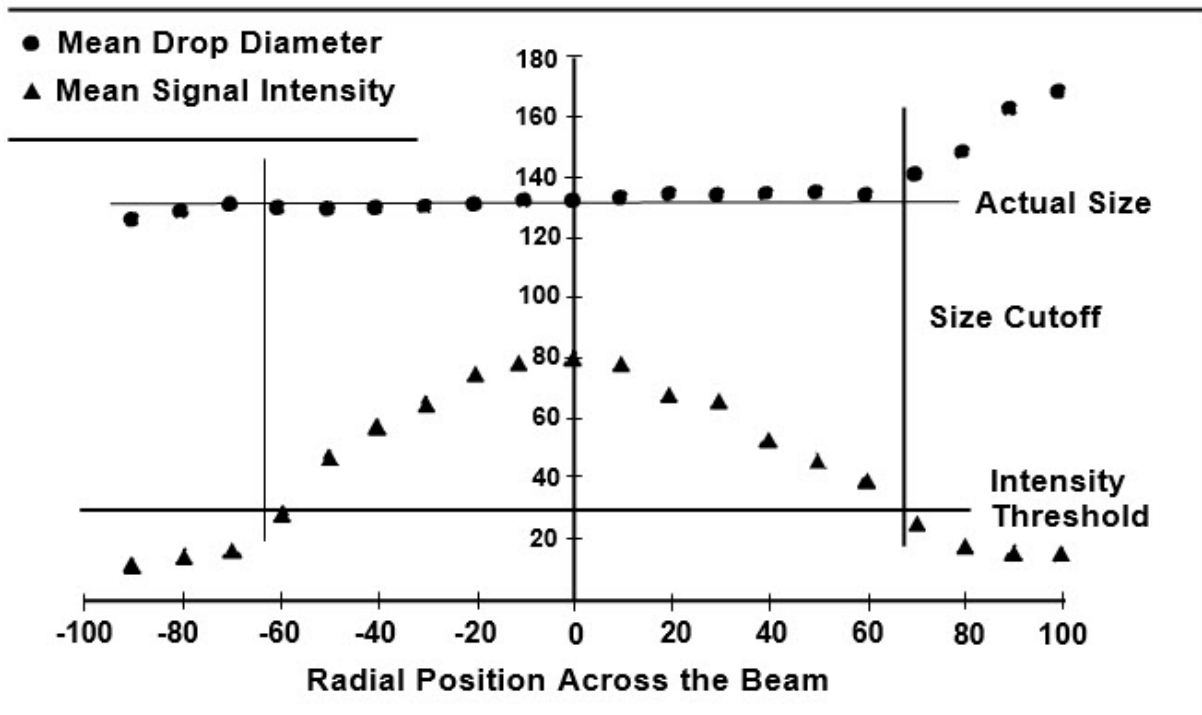


Figure A2.8. Plot showing the light scattering intensity and the measured drop size for a monodisperse drop stream traversed through the sample volume from one side to the other.

Numerous experimental evaluations of the method have been conducted. Figure A2.8 shows the results of traversing a monodisperse stream of droplets through the probe volume. The drops had a nominal size of 132  $\mu\text{m}$ . The plot shows the resulting light scattering intensity which is nearly Gaussian and the measured size as the stream is traversed from one side of the beam to the other (-100  $\mu\text{m}$  to +100  $\mu\text{m}$ ). The scattered light intensity profile will not be completely Gaussian in shape since the light scattering mechanisms change from one side of the beam to the other (more reflection detected on one side as a result of the location of the receiver). If a threshold intensity level is set (as shown in Figure A2.8) for each drop size class, the error in the measured size at the side with the reflective light scattering may be eliminated. For the “bad” trajectories, the measured size begins to deviate from the true value but setting a threshold signal amplitude level serves to exclude these readings. In principle, the adaptive threshold validation method limits the region of detection over the sample volume for each particle size class.

## **Examples of PDI Applications**

Numerous examples are available in the literature wherein the PDPA has been used to investigate spray characteristics in highly complex environments. This includes study of sprays injected into turbulent flow fields, reactive fuel sprays in swirl-stabilized combustors, characterization of rocket injectors in a high-pressure environment using cryogenic liquids, and the study of transient fuel sprays such as in spark ignition (SI) and diesel engines. The usefulness of the PDPA (now referred to as PDI instrument) in understanding various complex spray and combustion processes becomes apparent through the following brief description of some of the results that have been obtained to-date by various researchers.

### Spray Combustion Measurements

The development of the Phase Doppler Interferometer (PDI) has enabled the detailed measurement of drop size, velocity, number density and volume flux in realistic spray combustion environments [Bachalo et al. (1990); Edwards and Rudoff (1990)]. Chehroudi and Ghaffarpour (1991) investigated the effects of swirl and dilution air flow rates on the shape and stability of a kerosene flame on a model combustor with comparisons made of the non-combustible and combustible cases. The gas temperature was also measured within the flame using a thermocouple. Flow visualization showed non-uniformly-distributed separated finger-like regions of visible flames wrapped around the spray sheath. These structures were possibly due to large-scale eddies formed by the swirling

flow. At the center of the spray, drops with a reversed flow velocity were measured indicating a region of recirculation, Figure A2.9. In the burning case, no drops were detected in this region indicating that only vitiated air is recirculated toward the injector. At the uppermost end of the flame brush, a significant number of large drops were measured with velocities of approximately 10 m/s indicating that unburned drops were exiting the flame.

### Transient Fuel Sprays

Transient spray injection such as that used in Diesel and spark ignition engines shows some unique atomization characteristics. Diesel injection may take place into a relatively quiescent environment at pressures of approximately 15 atmospheres and at injection pressures of between 50 and 180 MPa. The important combustion parameters are the fuel penetration, mixing, and vaporization. These parameters depend upon the spray drop velocity and trajectory, the drop size distribution, and the turbulent gaseous flow field. The characterization of sprays having droplets of high velocity, small diameter, and high number density, which are typical of Diesel engines, is a challenging task, Harrington (1995). This is particularly true for smaller bore, light-duty, and medium-duty Diesel engines that utilize relatively short distances from the injector tip to the piston-bowl impact point. The combination of the above factors with high beam extinction in the spray core, and the need for a high-pressure optical chamber, leads to difficulties in all laser diagnostic methods. In spite of these challenges, the advanced frequency domain signal processors that are available for the PDPA has allowed for the reliable characterization of Diesel sprays.

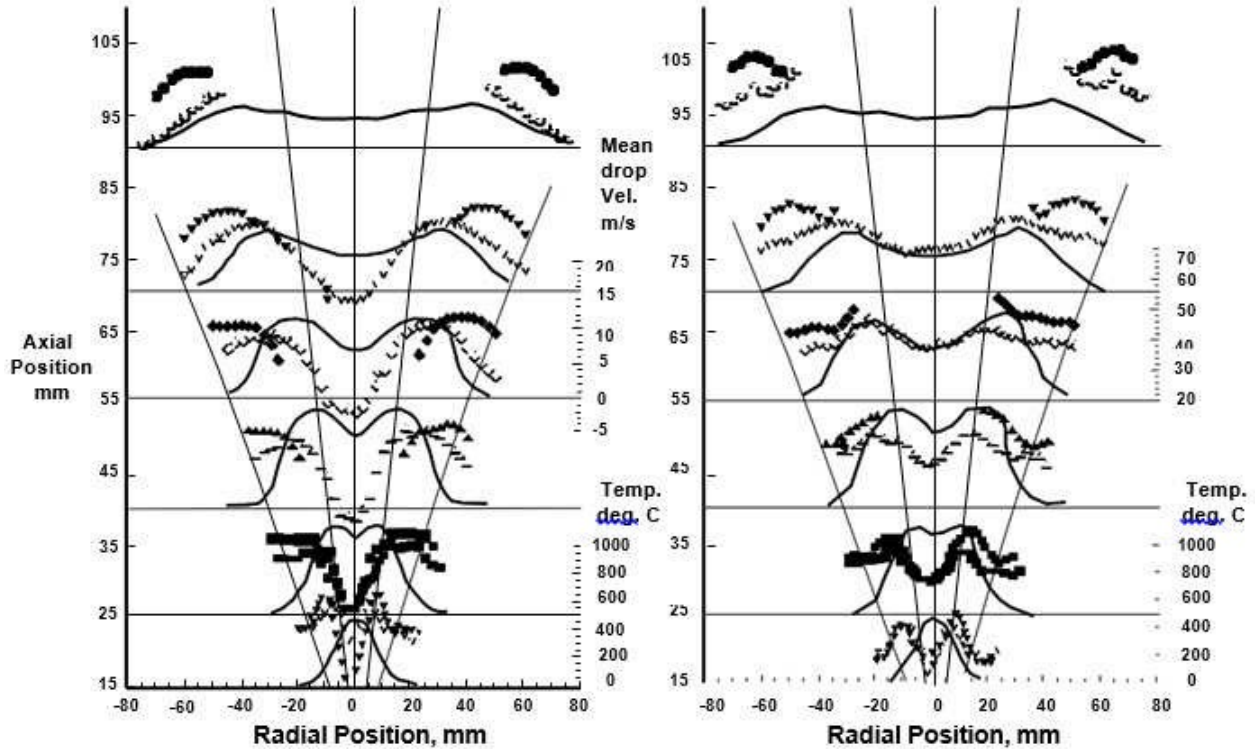


Figure A2.9. Drop size and velocity data obtained in a swirl-stabilized combustor comparing the results with and without combustion. The solid symbols are for the reacting case. Also shown is the gas temperature (solid line) obtained with a thermocouple (Courtesy of Chehroudi and Ghaffarpour [1991]).

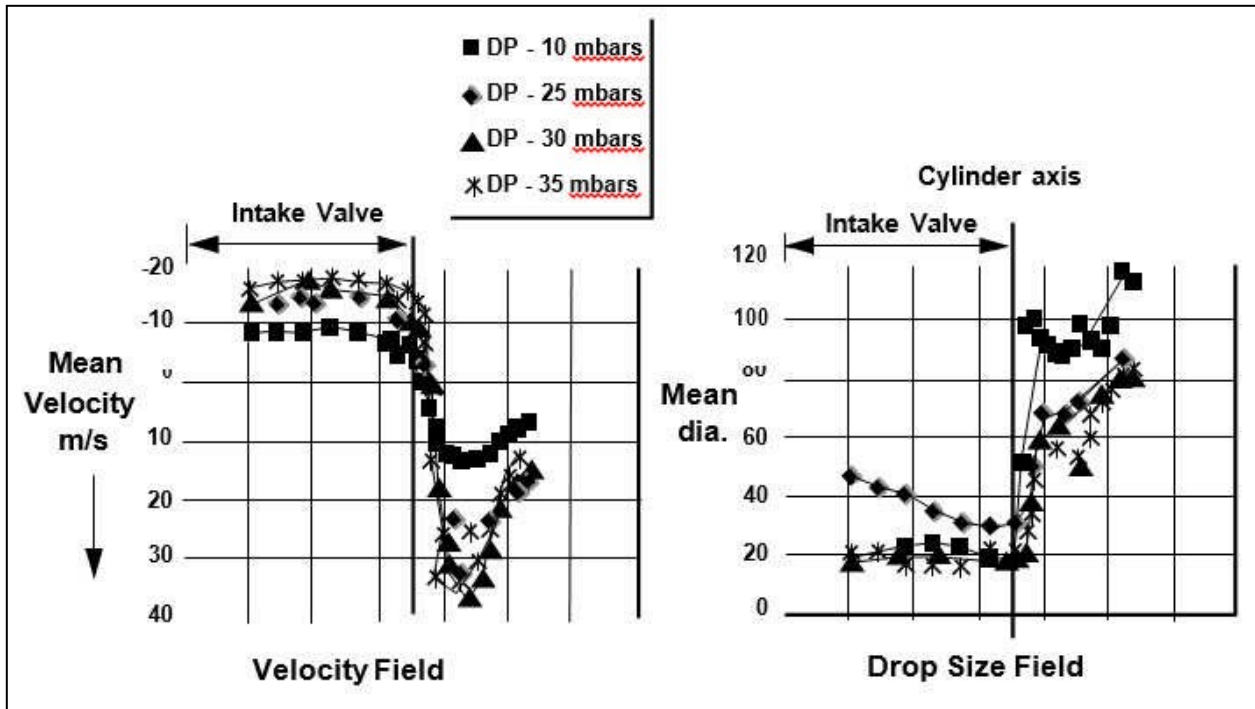


Figure A2.10. Air flow rate effect on drop size and velocity fields inside an SI engine cylinder.

As with Diesel engines, the atomization for spark ignition (SI) engines is highly transient and must be accomplished over a wide range of operating parameters. Vannobel et al. (1992) have used the PDPA to perform measurements in a gasoline spray inside the inlet port and downstream of the induction valve of a SI engine. Their interest was in studying quality of the air/fuel mixture and its dependence upon injection timing, injector position, and orientation within the manifold. The PDPA measurements were made inside the engine cylinder. The various curves in Figure A2.10 representing the different air pressures, illustrate the trajectories followed by the drops.



## Appendix III

### *Bibliography*

W. D. Bachalo, "Method for Measuring the Size and Velocity of Spheres by Dual-beam Light-Scatter Interferometry," *Applied Optics*, Vol. 19, No. 3, pp. 363-370, February 1, 1980.

W. D. Bachalo and M. J. Houser, "Phase Doppler Spray Analyzer for Simultaneous Measurements of Drop Size and Velocity Distributions," *Optical Engineering*, Vol. 23, pp. 583-590, 1984.

W. D. Bachalo and M. J. Houser, "Analysis and Testing of a New Method for Drop Size Measurement Using Laser Light Scatter Interferometry," NASA Contractor Report 174636, August, 1984a.

W. D. Bachalo, A. Brena de la Rosa, and R. C. Rudoff, "Diagnostics Development for Spray Characterization in Complex Turbulent Flows," 33rd ASME Gas Turbine and Aeroengine Congress and Exposition, Amsterdam, The Netherlands, June 6-9, 1988.

W. D. Bachalo and S. V. Sankar, "Analysis of the Light Scattering Interferometry for Spheres Larger than the Light Wavelength," *Proc. 4th Intl. Symp. on the Applications of Laser Anemometry to Fluid Mechanics*, Lisbon, Portugal, July 11-14, 1988.

W. D. Bachalo, R. C. Rudoff, and S. V. Sankar, "Time-Resolved Measurements of Spray Drop Size and Velocity," *Liquid Particle Size Measurement Techniques: 2nd Volume*, STP 1083, pp. 209-224, 1990.

W. D. Bachalo, E. J. Bachalo, J. M. Hanscom, and S. V. Sankar, "An Investigation of Spray Interaction with Large-Scale Eddies," AIAA 93-0697, 31st Aerospace Sciences Meeting and Exhibit, Reno, NV, January 11-14, 1993.

B. Chehroudi and M. Ghaffarpour, "Spray Drop size and Velocity Measurements in a Swirl-Stabilized Combustor," 35th International Gas Turbine and Aeroengine Congress and Exposition, Orlando, FL, June 3-6, 1991.

L. G. Dodge, "Comparison of Performance of Drop-Sizing Instruments," *Applied Optics*, Vol. 26, No. 7, April, 1987.

C. F. Edwards and R. C. Rudoff, Structure of a Swirl-Stabilized Spray Flame by Imaging, Laser Doppler Velocimetry, and Phase Doppler Anemometry, Proc. Twenty-Third Symp. (Intl.) on Combustion, Orleans, France, The Combustion Institute, pp. 1353-1359, 1990.

D. L. Harrington, PDA Measurement Considerations for Pulsed Air Assist and Diesel Fuel Sprays, Proc. 26th Annual Meeting of the Fine Particle Society, Chicago, IL, August 22-25, 1995.

K. M. Ibrahim, G. D. Werthimer, and W. D. Bachalo, Signal Processing Considerations for Laser Doppler Applications, Proc. 5th Intl. Symp. on the Application of Laser Techniques to Fluid Mechanics, Lisbon, Portugal, July 9-12, 1990.

K. M. Ibrahim, G. D. Werthimer, and W. D. Bachalo, Signal Processing Considerations for Low Signal to Noise Ratio Laser Doppler and Phase Doppler Signals, Proc. 4th Intl. Conf. on Laser Anemometry, Advances and Applications, Cleveland, OH, August 5-9, 1991.

K. M. Ibrahim and W. D. Bachalo, The Significance of the Fourier Analysis in Signal Detection and Processing in Laser Doppler and Phase Doppler Applications, Proc. 6th Intl. Symp. on the Application of Laser Techniques to Fluid Mechanics, Lisbon, Portugal, July 20-24, 1992.

K. M. Ibrahim, M. J. Fidrich, and W. D. Bachalo, Evaluations of an Advanced Real-Time Signal Processor System Using the Fourier Transform, Proc. 2nd Intl. Conf. on Fluid Dynamics Measurement and its Application, Beijing, China, October 1994.

S. V. Sankar and W.D. Bachalo, Response Characteristics of the Phase Doppler Particle Analyzer for Sizing Spherical Particles Larger than the Light Wavelength, Applied Optics, Vol. 30, No. 12, pp. 1487-1496, 1991.

S. V. Sankar, B. J. Weber, D. Y. Kamemoto, and W. D. Bachalo, Sizing Fine Particles with the Phase Doppler Interferometric Technique, Applied Optics, Vol. 30, No. 33, pp. 4914-4920, 1991.

S. V. Sankar, A. S. Inenaga, and W. D. Bachalo, Trajectory Dependent Scattering in Phase Doppler Interferometry: Minimizing and Eliminating Sizing Errors, Proc. 6th Intl. Symp. on the Application of Laser Techniques to Fluid Mechanics, Lisbon, Portugal, July 20-23, 1992.

S. V. Sankar and W. D. Bachalo, Performance Analysis of Various Phase Doppler Systems, Proc. 4th Intl. Congress on Optical Particle Sizing, Nuremberg, Germany, March 21-23, 1995.

S. V. Sankar, W. D. Bachalo, and D. A. Robart, An Adaptive Intensity Validation Technique for Minimizing Trajectory Dependent Scattering Errors in Phase Doppler Interferometry, Proc. 4th Intl. Congress on Optical Particle Sizing, Nuremberg, Germany, March 21-23, 1995.

Peter A. Strakey, Douglas G., Talley, Subra, V. Sankar, and W.D. Bachalo, "Phase-Doppler Interferometry With Probe-to-Droplet Size Ratios Less Than Unity. Trajectory Errors I.", Applied Optics, Vol. 39, No. 22, August 2000.

Peter A. Strakey, Douglas G., Talley, Subra, V. Sankar, and W.D. Bachalo, "Phase-Doppler Interferometry With Probe-to-Droplet Size Ratios Less Than Unity. Application of the Technique II.", Applied Optics, Vol. 39, No. 22, August 2000.

H. van de Hulst, Light Scattering by Small Particles, New York: Wiley, 1957.

Vannobel (1992), Private communications.